UNIVERSITY OF OKLAHOMA

GRADUATE COLLEGE

ANALYSING EYE TRACKING DATA IN A MULTI ELEMENT MOVING TARGET TRACKING SCENARIO: A DIRECTED WEIGHTED NETWORK APPROACH

A THESIS

SUBMITTED TO THE GRADUATE FACULTY

in partial fulfillment of the requirements for the

Degree of

MASTER OF SCIENCE

By

SAPTARSHI MANDAL
Norman, Oklahoma
2016

ANALYSING EYE TRACKING DATA IN A MULTI ELEMENT MOVING TARGET TRACKING SCENARIO: A DIRECTED WEIGHTED NETWORK APPROACH

A THESIS APPROVED FOR THE
SCHOOL OF INDUSTRIAL AND SYSTEMS ENGINEERING

BY

_____
Dr. Ziho Kang, Chair

_____
Dr. Randa Shehab

_____
Dr. Theodore Trafalis

Acknowledgements

Firstly, I would like to thank Dr. Ziho Kang for his constant support and guidance throughout these two years of my Masters' studies. Thank you very much for believing in me and giving me the freedom to pursue my own research ideas. I am indebted to you for your motivation and encouragement when the times where tough.

I would also like to thank Dr. Jerry Crutchfield and Dr. Angel Milan from FAA CAMI, OKC for their support for conducting the experiment at the FAA facility.

At the end, thank you MAA and BABA, though it's not possible to thank you enough for the sacrifices you have made to make me what I am today. I know your blessing are always with me; I am grateful to you guys for being there always.

Table of Contents

List of Tables

List of Figures

Abstract

Recent studies have shown that analysis of the eye tracking data is a viable way to understand the cognitive decision making process of people undertaking visual search tasks. As a result, its becomes important to develop new methods for analyzing the eye tracking data obtained in such scenarios. Visualization of data is a crucial stage in the analysis process. The prevalent eye fixation data visualization processes suffer from mainly two kinds of limitations, firstly; they are not efficient for large number of targets and secondly, they are unable to handle change in both the positions and the number of targets visible on the display. Another major shortcoming of the present methods' is the absence of quantitative metrics for advance analysis of the eye movement data.

The present study tries to address the above mentioned limitations by adapting the directed weighted network (DWN) methodology and its associated centrality metrics to develop a new visualization and analysis tool. A pilot study which simulated the realistic air traffic control task environment was performed to demonstrate the developed methodology. The results obtained are very promising, as the method was able to identify the important targets (aircraft) interrogated by the air traffic controller based on different time frames. The obtained result lays the first stepping stone in the development of an effective data visualization method and also quantitative metrics for analyzing complex eye movements for a multi-element tracking task.

Key words: Eye tracking, Multi-element moving object, Air traffic control, Directed weighted networks, Centrality metrics,

Chapter 1: Introduction & Literature Review

1.1 Eye tracking & its applications

Previous researches have shown that eye tracking technology can be a very useful in understanding human cognitive process. Just and Carpenter (1976) in their work showed that, while performing a given task, there lies very high correlation in the cognitive process happening in our mind and the way we observe things during that task execution. In the last few years, with rapid technological advancement, eye tracking technology has become available to people outside the research labs in the market place also, as a result, this technology has been applied in many diverse domains.

Aula, Majaranta, and Räihä (2005) had applied eye tracking data in evaluating the usability of websites. In the domain of driving the eye tracking technology has been applied to analyze driver's scanning behavior (Underwood, Chapman, Brocklehurst, Underwood, & Crundall, 2003). Holland and Komogortsev (2011) showed that eye fixation strategy can be used in analyzing the pattern in which people perform a reading task. Kang and Landry (2014), Mandal, Kang and Milan (2016) have used the eye tracking research in the field of air traffic control. They tried to analyze the fixation strategy of air traffic controllers' that happened during scanning the radar screen. Kang and Landry (2015) showed that the eye tracking technology can also be used to evaluate the human performance in tasks which involves tracking objects in a dynamic scenario.

While implementing the eye fixation research, after the eye fixation data (a pixel based vertical and horizontal co-ordinates of the eye fixation location) is collected, it is superimposed on the objects present on the visual display. Given the eye tracking data the main objective lies in understanding two things. Firstly, whether or not any fixation has occurred on the object of interest, present on the visual display, under consideration. Secondly, in what other the different objects are fixated upon. As a result, one of the basic but foundational step in the eye tracking research is the process of mapping eye fixations to object of interest present on the display. As per Poole, Ball, and Phillips (2005) one of the efficient way for developing this mapping structure is to create an area of interest (AOI), a geometrical boundary, surrounding the object of interest on the visual display.

1.2 Area of Interest (AOI)

One of the preliminary concept of AOI was demonstrated by creating a rectangular boundary around a collection of simple dots which are moving in time (Howe, Drew, Pinto, & Horowitz, 2011). For the analysis purpose the AOI can be used to replace the object of interest under consideration itself; in other words, eye fixations occurring within the AOI boundaries can be treated as eye fixations falling on the object under consideration. This concept of the application of AOI for replacing the object itself proves very efficient in scenarios where the objects have multiple moving elements; since considering each element separately for analysis makes it a very tedious job. Figure 1 represents the concept of an AOI, where the

black box surrounding all the individual orange dots represents an AOI and for analysis sake we can replace the individual orange dots present within the box using the black boundary of the box itself. This approach becomes valid since the orange dots are very close to each other and as a result can be considered as a single object of interest. Apart from that they are also moving with respect to time. Thus considering the AOI proves to be more efficient in such scenario as far as the mapping of the eye fixations are concerned.

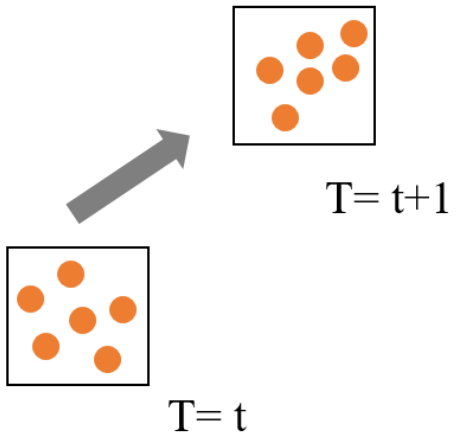

Figure 1: Example of an AOI

Even though the concept of creating a rectangular boundary around the object of interest is quite easy to conceptualize, the difficulty arises when the objects of interest are moving with time, changes their shape with time and also consist of multiple elements.

A practical task which involves the objects of interest having the above mentioned structural characteristics is the work of the air traffic controller (ATC) while managing the flow of the air traffic. The ATCs have to detect and guide multiple aircraft (visible on their radar display) through their trajectories and they are also required to ensure that there is no possible conflict among the various aircrafts for safety reasons.

1.3 Multi-element moving object

Multi-element moving object literally means the object under consideration is made up of multiple individual elements are but moving together as a single entity (figure 2). Figure 2 shows a typical representation of an aircraft as visible on the ATC's radar display. As we can see that the representation consists of various elements namely, data block (containing the information of the aircraft's name, speed, altitude and destination), vector line (showing the direction in which the aircraft is moving), target location (aircraft's positon co-ordinate on the display) and lastly the line joining the target and the data block. The vector line length is proportional to the aircraft's speed thus its length can vary with change in speed. The position of the data block can be changed by the ATC.

The aircraft shown in figure 2 can be represented with a simple representation as shown in figure 3. The figure 3 shows how the shape of the object can change with passage of time.

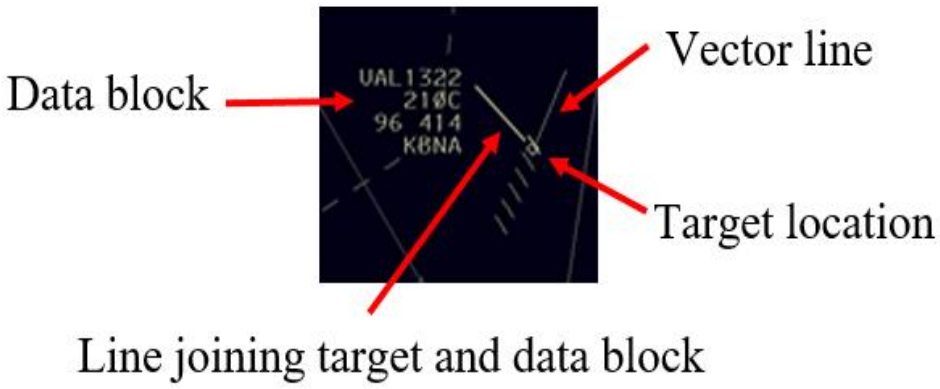

Figure 3: Aircraft visualization on the ATC visual display

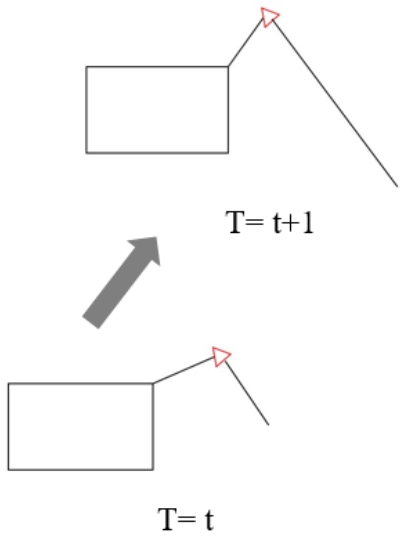

Figure 2: Multi element moving object

1.4 Dynamic and flexible AOI

For the case of mutli-element moving objects many researchers have considered various types of AOIs, e.g. a rectangular AOI to represent an aircraft (Kang & Bass, 2014), circular, triangular and rectangular AOIs to approximate an aircraft (Mandal & Kang, 2015). Both the researches have used AOIs which move along with the object of interest (dynamic AOIs) but they were fixed as far as their shape was concerned. Although creating a dynamic AOI and approximating the object of interest helps us in analyzing the eye fixations on moving multi-element objects, there are major obstacle in its practical implementation. The shape of the AOI is very much dependent on the shape of the object under consideration as a result a static AOI, in terms of shape, cannot address the issue of multi-element moving object where the shape of the objects can change drastically with time. Thus, we require to create an AOI which is both dynamic in nature and also is flexible in terms of the shape also.

Figure 4 represents such a case where the AOI is both moving with time and also changing its shape as per the change in the object is representing. The orange border represents the AOI for the aircraft representation. In the figure the AOI is the convex hull of the co-ordinate points of the various element's used to the represent the aircraft. Once the mapping of the eye fixations is completed, the next step in the eye tracking research is the visualization of the obtained results.

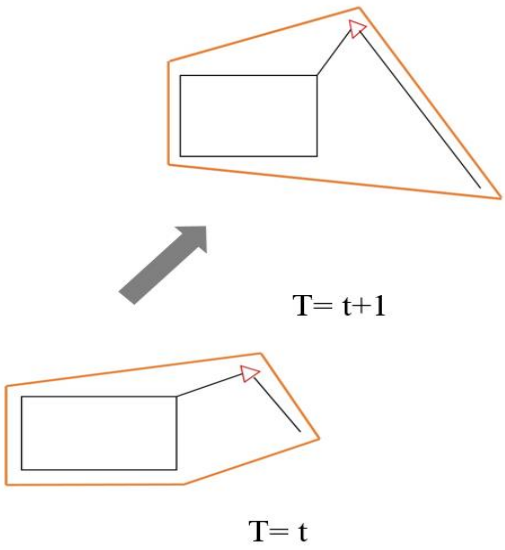

Figure 4: Multi element moving object with its AOI

1.5 Visualization of eye fixation data

Visualization of eye tracking data plays a very important role in the field of eye tracking research. The visualization technique proves to be very helpful in understanding the spatio-temporal distribution of the eye fixation. Apart from that, on preliminary visual investigation (with very little or no computational cost involved), it also reveals various complex relationships existing within the data (Blascheck et al., 2014).

Various kinds of visualization techniques have been developed so far; and they capture different attributes of the eye tracking data. All the prevalent visualization methods can be classified into three major classes namely, point based, AOI based and a combination of both (Blascheck et al., 2014).

The point based approaches visualizes the actual co-ordinate locations of the eye fixation points. As per Blascheck et al., (2014) the point based approaches can be further subdivided into three categories namely, temporal (Grindinger, Duchowski, & Sawyer, 2010), spatial(Goldberg & Helfman, 2010) and spatio-temporal (Duchowski, Price, Meyer, & Orero, 2012).

One of the techniques within the temporal point based approach is the timeline visualization (Grindinger et al., 2010); where the co-ordinate points of the eye fixations are represented on a two dimensional axis with one axis representing the change in time. Attention maps, a point based spatial visualization techniques, aggregates the eye fixations data over time to represents those areas of the display which have garnered comparatively more attention (Blignaut, 2010). The technique of scanpath visualization falls under the third category of point based spatio-temporal visualization approach. In this technique, consequent eye fixations points (represented as circles, whose radius is proportional to the fixation duration) are connected with a line (saccade line), the direction of which shows the order of the fixation that's has occurred (Lankford, 2000).

The point based approaches have their own advantage by being computationally less expensive to implement but they are unable to handle scenario where the objects of interest are dynamic in nature and also change their shape and size with passage of time. Thus, they are not suitable for visualizing the eye fixation data obtained from such a scenario having mutli-element moving objects of interest. The AOI based approach is deemed more suitable for addressing the particular

challenges of having mutli-element moving objects scenarios (Kang & Landry, 2015).

The AOI based approaches mainly deal with the temporal aspects of the fixation over the AOIs (Kurzhals, Heimerl, & Weiskopf, 2014) or the relational aspect among AOIs (Mandal et al., 2016). The temporal AOI based visualization approaches (parallel scanpath plotting, AOI river plots) works similarly like their analogous counterparts in the point based category. In this approach also the time is represented on one of the two axes and the other axis shows how the AOIs are fixated upon at various intervals of time (Raiha, Aula, Majaranta, Rantala, & Koivunen, 2005). The temporal AOI based approach losses their efficiency when the number of AOIs increases to large values.

The relational AOI based approaches mainly deals with visualizing the relationship that exists between the various AOIs being fixated upon. This approach has two main categories namely, matrix based and graphical based. The matrix based approaches shows the AOI transition matrix depicting the order of movement of the eye fixation between various AOIs under consideration (Goldberg & Kotval, 1999). This approach also suffers from similar limitation as the temporal approaches do; since with large number of AOIs, the size of the transition matrix becomes very large, it becomes very complex to the understand the relationship among the AOI states with just naked eye investigation.

The other approach within the domain of relational AOI based visualization is the graphical approach; where the node of the graph represents the AOIs and the

edges represents the transition of the eye fixation data (Tory, Atkins, Kirkpatrick, Nicolaou, & Yang (2005); Mandal et al., (2016)). The graphical approach has the capability to handle very large number of AOIs. Apart from that this approach can be utilized to represent various attributes of the eye fixation data (eye fixation duration on AOIs, transiting among AOIs, fixation number on AOIs, relative importance of AOIs) by utilizing the various structural attributes of a graph e.g. node size, node colour, edge thickness etc. The graphical approach also lets us develop advanced quantitative metrics, which is required to understand complex eye fixation strategies obtained from tasks which involve tracking dynamic multi-element moving objects.

.

Chapter 2: Objective

2.1 Objective

The objectives behind undertaking this research endeavor is three fold. The first objective is to develop a new analysis framework for the eye tracking data obtained in a multielement moving object tracking scenario.

The second objective is to develop a new visualization technique for representing the eye fixation data obtained in the above mentioned scenario.

Lastly the third objective is to develop advanced quantitative metric to further aid the analysis. The metrics thus developed will provide a quantitative framework which will help us in understanding the underlying cognitive process of the participant's involved in the task; and also will proving a framework to compare the eye fixation strategy among various participant

Chapter 3: Methodology

This chapter describes the methodology used to develop the directed weighted network (DWN) representation of the eye tracking data of the ATC, obtained from the simulation experiment performed at the FAA CAMI in OKC. Figure 5 represents the overall algorithmic flowchart, showing different steps, of the methodology used. The initial step consists of the simulation experiment, where we conduct a simulation experiment and obtain relevant data for the subsequently developing the module 1, module 2 and module 3 in the given order. The details of the various stages of the flowchart have been described in the following subsections.

3.1 Simulation experiment

3.1.1 Experimental setup & data collection

The following section provides the details the of the experimental setup and the data collected from it.

Participants: In total, eye tracking data of nine retired ATCs was collected. To test the proposed algorithm, as a pilot study, only one ATC's eye tracking data was analyzed. The analysis of the eye tracking data of the other eight participants is still in progress.

Apparatus: *Hardware specifications*: For displaying the simulated air traffic movement a 19.83 × 19.83-inch monitor (2048 × 2048-pixel active display area)

was used. For capturing the eye tracking data, FaceLab 5 eye tracker system (Ekstremmakina.com, 2016) with a sampling rate of 60Hz was used.

Software specifications: Kongsberg-Gallium I- Sim software**,** internally developed and used by the Federal Aviation Administration (FAA), was used to generate aircraft traffic simulation scenario, whose refresh rate was 1 second. Eyeworks software (Eyetracking.com, 2016) was used to process the raw eye fixation data collected by FaceLab 5.

Both the hardware and software were provided by the FAA Civil Aerospace Medical Institute (CAMI) in Oklahoma City. The data obtained from the experiment has been described in detail in subsequent subsections.

Scenario: This consisted of a **s**imulated air traffic scenario of 20 minutes in duration with 20 aircraft on average on the display screen. Figure 6 shows a snapshot of the scenario used for the experiment. The direction of the movement of the aircraft is shown in yellow dotted lines e.g. aircraft labeled as G is moving eastward, whereas aircraft named A is moving westward. The actual simulation video didn't have these yellow letters and lines to maintain a high fidelity simulation scenario.

Task: The task for the participants involved controlling the air traffic in a low altitude en-route airspace using a simulated ERAM system (also provided by FAA). In addition to the ATC there were two pseudo pilots also, who were involved in the experimental process. Their job was follow the instructions of the ATC (given

through voice commands) and do the necessary maneuvering of the aircrafts. Simulated radio connection was used to perform all the above mentioned communications among the ATC and the pseudo pilots.

The data collection process involves collection of two data files namely, (1) Air traffic simulation data file and (2) Eye fixation data file. The following section provides detail description of these two data files.

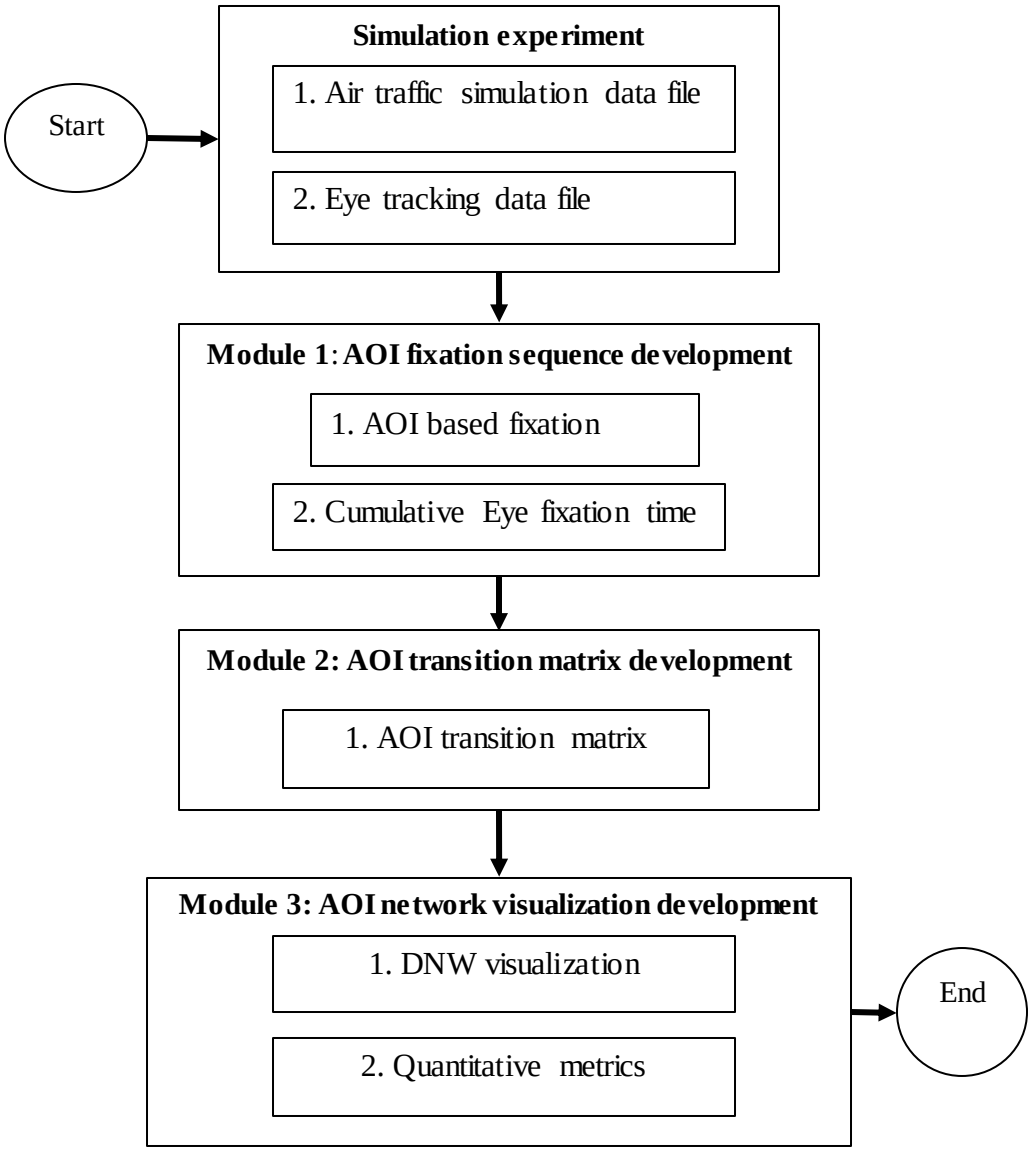

Figure 5: Algorithmic flowchart for various modules generated from simulation experiment data

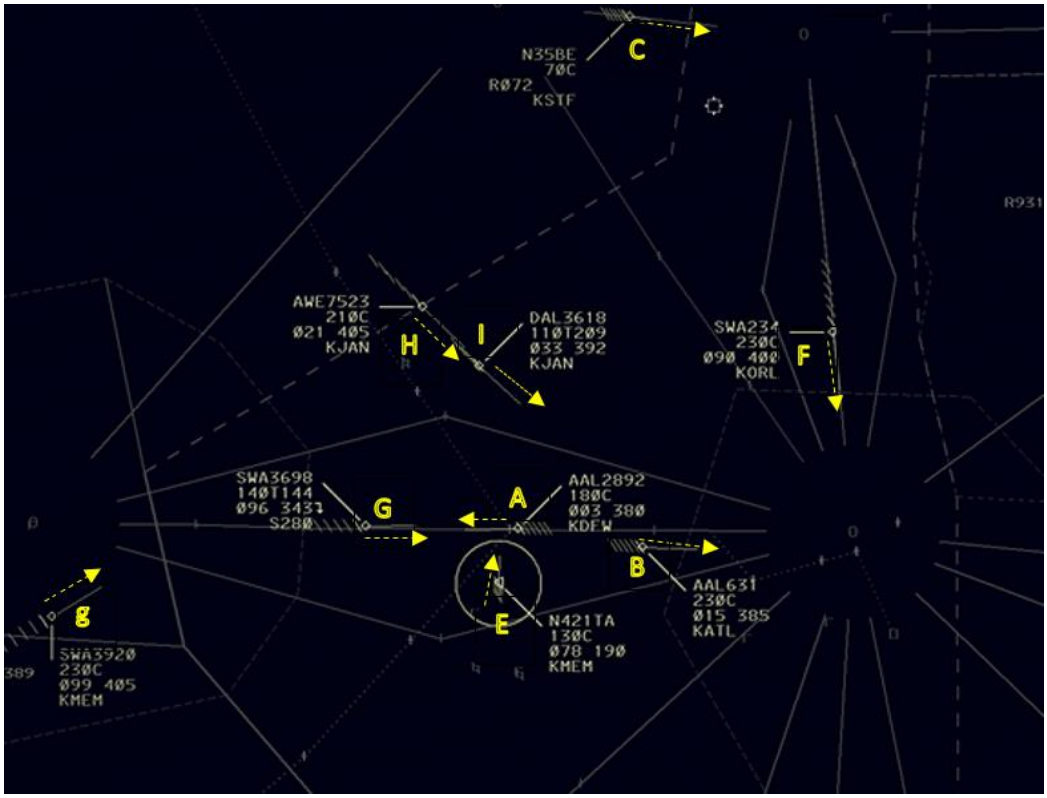

Figure 6: A snapshot of the simulated scenario used in the experiment

3.1.2 Air traffic simulation data file

The air traffic simulation data file consists of the relevant information w.r.t the different aircrafts visible on the radar screen during the experiment duration. Table 1 shows a sample of the Air traffic simulation data file. From the table we can see that the data file shows information w.r.t the aircraft coordinates for various time values, and other relevant details of the aircraft representation used for the simulation. In Table xx, the first two columns namely, scenario time and time of the day shows the time that has elapsed from the start of the experiment and the actual time of day, respectively. The third column represents the aircraft's code

name. The fourth column named "target" shows the horizontal (X Pos.) and vertical (Y Pos.) coordinates of the targets (aircraft in this case) in pixel format. The fifth column consist information w.r.t the "data block" (a rectangular block representation containing information about speed, altitude, destination of the corresponding aircraft. The data block information consists of two subparts, firstly top left corner coordinates of the data block and secondly the bottom right corner coordinates of the data block. The last column provides the end position coordinates of the vector line in pixel unit.

Table 1: A sample air traffic simulation data file

Scenario time	Time of the day	Aircraft code	Target		Data Block location				Vector line end points	
					Top left		Bottom right			
			X Pos.	Y Pos.	X Pos.	Y Pos.	X Pos.	Y Pos.	X Pos.	Y Pos.
00:01:02	9:4:33	AWE7523	985	938	1045	920	1134	995	950	884
00:01:02	9:4:33	DAL3618	545	1240	560	1280	631	1355	592	1248
00:01:03	9:4:34	AWE7523	986	939	1045	920	1134	995	950	884
00:01:03	9:4:34	DAL3618	545	1005	560	1280	631	1355	592	1248

3.1.3 Eye fixation data file

The eye fixation data file consists information w.r.t the spatial location (horizontal and vertical co-ordinate points) and the time duration of each of the eye fixations made by the ATC during the experiment. Table 2 represents a small snapshot of a sample eye fixation data file. The first column represents the horizontal axis (X Pos.) and second columns shows the vertical axis (Y Pos.) pixel-

coordinates of the eye fixations. The third and fourth columns represents the start and stop time of an eye fixation respectively. The duration of the concerned eye fixation is shown in the fifth column.

Table 2: A sample eye fixation data file

X Pos. (pixels)	Y Pos. (pixels)	Start time (secs)	Stop time (secs)	Duration (secs)
500	457	0.30	0.53	0.23
440	358	0.60	0.85	0.25
652	550	1.10	1.84	0.74
829	924	2.12	4.28	2.16

3.2 Module 1: AOI fixation sequence development

After the two data files have been obtained the next stage is the development of Module 1. Module 1 consists of the development of the AOI based fixation sequence. The details regarding the development of this module has been already published in Kang et al., (2016); and this section briefly describes the same. Before the AOI fixation sequence can be developed, using the air traffic simulation data and the eye fixation data, few other things that needs to be considered are as follows:

i. How to develop the AOIs for the aircraft's present in the simulation scenarios?

ii. How to take into account the accuracy issues of the eye tracker used in data collection?

Mandal & Kang, (2015) undertook a study exploring various different geometrical shapes acting as an AOI and its effect on the eye fixation data attributes (number of eye fixations, duration of eye fixations). The geometrical shapes considered by them was namely, circle, rectangle and triangle. Mandal & Kang, (2015) found no statistically significant difference, w.r.t the eye fixation data attributes, between the various geometric shapes. Although, one particular thing to notice was that the various different AOI shapes considered were insensitive to the changes in the shape of the aircraft's. In other words, the AOI didn't change shape with change in the shape of the AOIs because the size of AOIs considered were big enough to accommodate all shape variation of the aircraft's (this is relevant only for the simulations scenario considered by Mandal & Kang, (2015)) without changing their own shape. In general, it is difficult to assess what all possible shape variations might occur w.r.t the aircraft's during a real life setting, thus the approach where the AOIs remain fixed in the shape is not applicable for the present study. Therefore, to address the issue highlighted in (i), for the present study the shape of the AOI, named convex AOI, was developed by calculating the convex hull (Barber, et. al.; 1996) of the set of points representing the aircraft under consideration.

Figure 7 represents a typical representation of an aircraft in the simulation scenario (represented in black). The figure also shows a tightly fitted convex hull AOI (shown in dotted green), called convex AOI henceforth, and also a loosely fitted convex AOI (shown in green). From the figure we can see that the loosely

fitted AOI has some gap from the actual boundary of the aircraft representation. Kang et al., (2016) has described this gap as the AOI gap tolerance value or AGT VALUES is short. The AGT VALUES was considered to address the issue highlighted in (ii). The FaceLab 5 eye tracker system that was used for the data collection (Ekstremmakina.com, 2016) had a visual angle accuracy in the range of 0.5^0-1^0. The size of the display, used for scenario representation, also contributes towards the accuracy of the eye tracker system; size of the display is inversely proportional to the accuracy of the eye tracking data thus obtained. Due to the accuracy issue, many of the eye fixation positions noted are not correct w.r.t their vertical and horizontal pixels' co-ordinates.

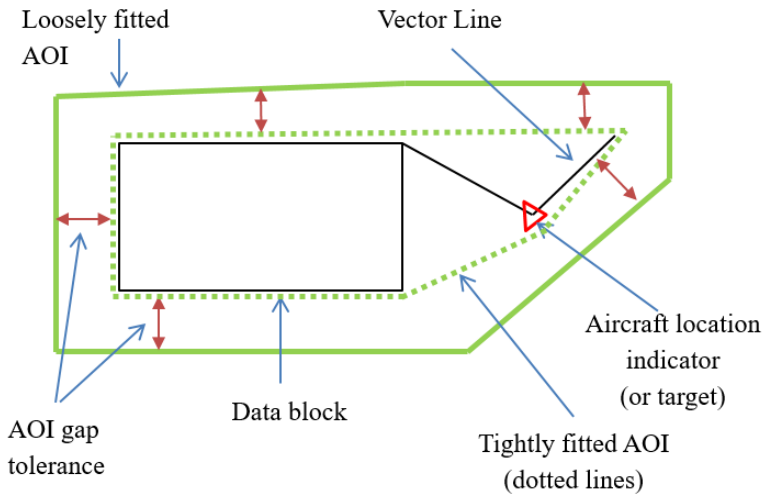

Figure 7: A sample aircraft representation with its convex hull AOI. *Figure adapted from Kang et al., (2016).*

The next step in the process of the AOI fixation sequence development is the mapping of the eye fixation data with AOIs. Kang et al., (2016) described this mapping process as function, called AM (AOI Mapping), mapping the elements of the eye tracking data set to the elements of the AOI set. Mathematically it can be written as follows:

$$AM : E \rightarrow AOI \quad \ldots (1)$$

Where,

AM is the AOI Mapping function,

E is the eye fixation data set (domain of the AM function)

AOI is the set of AOIs (range of the AM function).

If an eye fixation falls within the boundary of an AOI then that particular eye fixation is mapped to that AOI. As we know, the AOIs under consideration are moving on the display, as result there can arises cases where an eye fixation falls within the overlapped region of the more than one AOI. Figure 8 represents the two different mapping scenarios. Figure 8 (a) represents the case where a given eye fixation falls within the boundary of only one AOI and figure 8 (b) shows the scenario where the given eye fixation falls in the overlapped region of many AOIs (three AOIs in this case). Another scenario can also occur where the eye fixation doesn't fall inside any AOI boundary; in that case it is mapped to a non AOI, in the present case the non AOI is shown by "-1".

After each of the eye fixations made by the ATC is mapped to their corresponding AOI/AOIs we obtain the raw AOI fixation sequence. Before we start calculating the relevant eye tracking data metrics, we need to convert the raw AOI fixation into collapsed AOI fixation sequence data. Table 3 shows a sample raw AOI fixation sequence and its corresponding collapsed version. The collapsed fixation is obtained by deleting the multiple consecutive occurrence of the same AOI in the raw fixation and replacing it by only a single instance of the AOI.

Table 4 represents a sample collapsed AOI fixation sequence data. The first column named "In/Out flag" takes only binary values (either 0/1). O represents that the fixations/ fixations under consideration occurred outside any AOI boundary, whereas 1 means that the corresponding fixations occurred inside atleast one AOI boundary. The second column named "Eye fix. Index" shows the list of consecutive indexed eye fixation points that occurred either outside the AOI boundary or all together on the same AOI/ AOIs boundary. The third column named "# of eye fix." counts the number of eye fixations present in the "Eye fix. Index" column of the same row. The fourth column "AOI name list" shows the AOI/ AOIs that has been mapped to the eye fixation/fixations shown in the column "Eye fix. Index". The last column named "Eye fix. time duration (secs.)" represents the amount of total eye fixation duration that occurred on the mapped AOI/ AOIs.

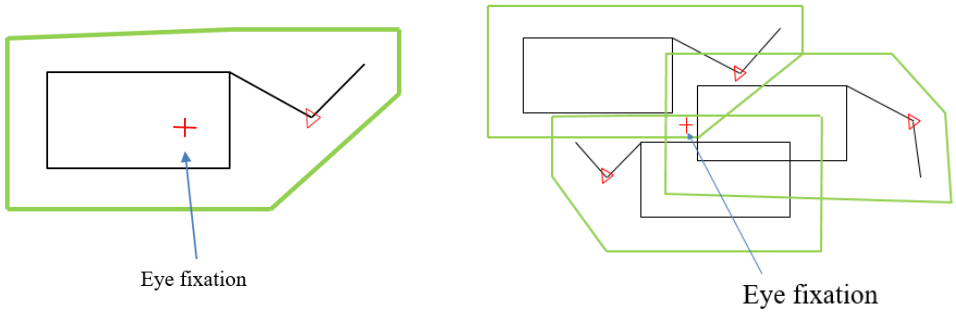

(a) (b)

Figure 8: Mapping of eye fixation with AOIs (a) Mapping with single AOI (b) Mapping with multiple AOIs

Table 3: Example of raw and collapsed AOI fixation sequence

Raw AOI fixation sequence	Collapsed AOI fixation sequence
AABBCB(A,D)	ABCB(A,D)

Table 4: Sample AOI fixation sequence output

In/out flag	Eye fix. Index	# of eye fix.	AOI name list	Eye fix. time duration (secs.)
1	1	1	A	0.2
0	[2,3,4]	3	-1	1.2
1	5	1	[H,I]	0.8
1	[6,7]	2	G	0.5

Kang et al., (2016) called the various rows of the "AOI name list" column (table 4) as the mapped AOI set (MA set); e.g. the MA set for the 1st row is MA_1={A}, similarly, MA_2={-1} and MA_3={H,I}. Thus, we can see the cardinality

of MA set varies from ϕ (for MA_2= {-1}) to 2 (MA_3={H,I}). Kang et al., (2016) studied the frequency distribution of the MA sets having various cardinalities for different levels of AGT values ranging from 5 to 100 pixels. The authors calculated the optimal value of the AGT using the following equation:

$$AGT_{optimal} = \underset{AGT \in \{5,10,15,\ldots,100\}}{\arg\max} [\, freq(c) \mid c = 1] \quad \ldots (2)$$

Where,

c is the cardinality of the MA set.

AGT is the AOI gap tolerance value used

From the equation 2 we can see that the optimal AGT value is that particular AGT value where the frequency of the mapped AOI set, of cardinality 1, reaches its maximum. Figure 9 (a), (b) and (c) shows the variation of the frequency of the mapped set of various cardinalities for different values of the AGT for three different scenarios. The specific characteristics of the three scenarios are explained in detail in Kang et al., (2016) . As we can see from the figure that the maximum value of the frequency of the MA set, having c=1 for all the three scenarios, is reached around AGT value of approx. 40 pixels. Therefore, for the present study AGT value of 40 pixels has been used to develop the convex AOIs and subsequently the AOI fixation sequence.

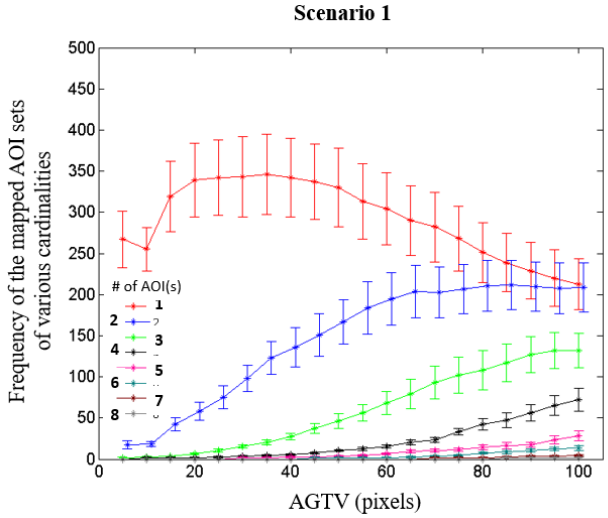
Scenario 1
Frequency of the mapped AOI sets of various cardinalities
# of AOI(s)
1
2
3
4
5
6
7
8
AGTV (pixels)

(a)

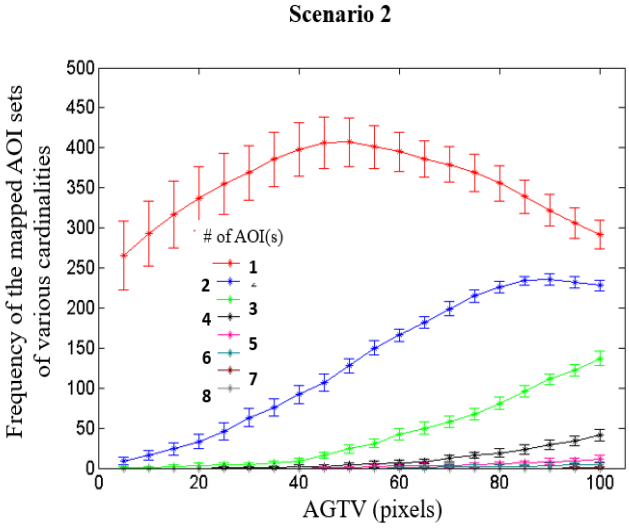
Scenario 2
Frequency of the mapped AOI sets of various cardinalities
# of AOI(s)
1
2
3
4
5
6
7
8
AGTV (pixels)

(b)

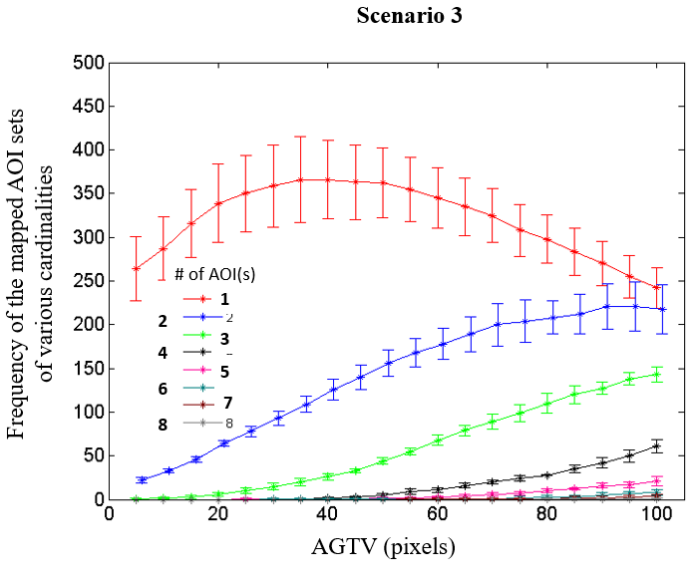

(c)

Figure 9: Frequency distribution of mapped AOI set, of various cardinality, for different AGT values (a) scenario 1, (b) scenario 2, (c) scenario 3. *Adapted from (Kang et al., 2016).*

3.3 Module 2: AOI transition matrix development

Once the AOI fixation sequence has been developed, the next step involves development of module 2, i.e. the development of the AOI transition matrix from the above mentioned sequence obtained as output from module 1. In order to understand the development of the AOI transition matrix in detail, let us consider a sample example of AOI fixation sequence: "**AB(AC)DABDCA**". In the given sample sequence, we can see that, the first fixation occurred on AOI named 'A' then 'B' then on both 'A' and 'C' simultaneously and then 'D', 'A', 'B', 'D', 'C' and lastly on 'A'. The particular representation ("AC") shows that the eye fixation has occurred on the overlapping region of AOI named 'A' & 'C'. For the present research endeavor all such overlapping AOI cases (e.g. "AC") are considered as separate transition states different from the elemental AOIs (e.g. "A" & "C") contributing to the formation of the overlapped cases. Another point to be noted is that the transition matrix is developed from the AOI based sequence, which is again dependent on the eye fixation data. The transition matrix resulting from this strategy and above mentioned example sequence is shown in Table 5.

For the present case, as described in section 3.1.1, we have considered a simulated experimental scenario where the AOIs were moving on the display and their shape can also be changed by the onlooker; as a result of this dynamic nature of the AOIs very often situations can arise where various AOIs are overlapping with each other. Thus such a scenario, with various possible overlapping situations,

can give rise to a very large number of possible transition states. For a general scenario, if we do not know the trajectories of these moving AOIs beforehand, it becomes computationally very expensive to take into account all possible transition states. Another point to be noted here is that even though there might be many possible situations of overlapping AOIs on the display but those states may not be fixated upon by the onlooker; as a result, these scenarios will not appear on the AOI based fixation sequence. Therefore, most of such states will have zero values associated with them in the transition matrix representation as a result these states will have no impact on the relevant metrics thus developed from the transition matrix. More importantly since our major purpose is to understand the cognitive strategy of the onlooker, rather enumerating all possible AOI states, it is more judicious to take into account only those states which are viewed or fixated upon by the onlooker. Thus, this approach of limiting the transition states to the states observed in the AOI based sequence reduces the computational cost involved in developing the transition matrix. In module 2 we also extract the cumulative eye fixation time spent on each of the transition AOI states.

Table 5: AOI transition matrix developed from the example AOI fixation sequence

		To				
		A	**B**	**C**	**D**	**A,C**
From	**A**	-	2	0	0	0
	B	0	-	0	1	1
	C	1	0	-	0	0
	D	1	0	1	-	0
	A,C	0	0	0	1	-

3.4 Module 3: AOI network visualization development

After the transition matrix has been developed the next step is the **module 3** which involves developing the network representation of the transition matrix data and subsequent quantitative metric development from the developed network. The following sections demonstrates bot these processes.

3.4.1 DNW visualization

The matrix structure as obtained in table 5 shows that we can represent it in the form of a Directed Weighted Network (DWN) in which the nodes of the network can represent the AOIs and the edges of the network can be used to represent the transition between the AOIs. If we consider two arbitrary nodes (AOIs) named 'i' and 'j' then we will construct an edge joining them if the transition value $t_{ij} > 0$, where t_{ij} is the cell value of the i^{th} row and j^{th} column in the transition matrix. The value of t_{ij} will represent the weight of the edge. The direction of the edge will be from the 'From' AOI state to the 'To' AOI state. The origin and the destination of any particular eye fixation transition is shown by the direction of

the edge that connects any two nodes. The edge weights represent the total number of transitions that occurred in that direction. Another important edge attribute, that is used to aid the visualization process, is its thickness. In the present study for any given edge's, its thickness is made proportional to the number of transition that happened in that direction.

The other important structural aspect of the network visualization process are the nodes and their associated attributes such as colour and size. In the present design methodology, the size of the node has been made proportional to the node weight and its colour is dependent on the amount of the cumulative eye fixation time that occurred on it. A node having larger cumulative eye fixation time value associated with it is represented in more reddish colour and vice-versa; whereas nodes with low values of cumulative eye fixation time on it are represented with more yellowish colour and vice-versa. Thus, in a given network the nodes having relatively high values of cumulative eye fixation time duration on them will have reddish colour and nodes having relatively small values will have yellowish colour. Figure 10 represents the DNW representation of the AOI transition matrix shown in table 5. From the figure we can see that the nodes having higher input/ output eye fixations (in any general setting the number of input and output eye fixations are same) are relatively bigger in size. The thickness of the edge is proportional to its respective weights, e.g. the thickness of the edge from node "A" to node "B" is more compared to the other edges in the network visualization. From the figure 10 we can also see that the nodes are given different colour. For the given figure we

can see that the node named 'A' (red in colour) has the highest cumulative eye fixation duration associated with it whereas the node named 'C' and 'A,C' (yellow in colour). have the lowest eye fixation duration associated with it.

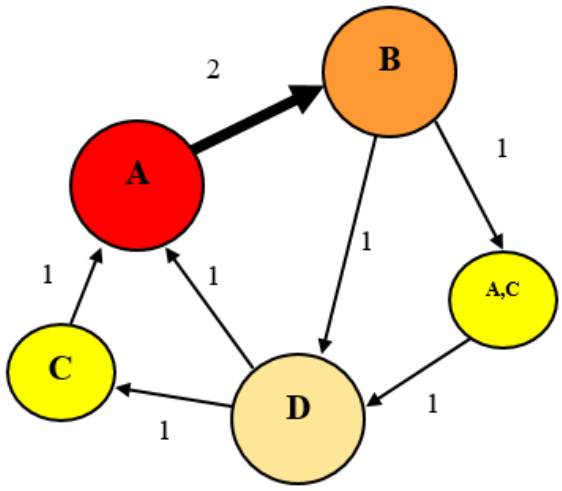

Figure 10: DNW representation of AOI transition matrix shown in table 5

3.4.2 Quantitative metrics

After the attributes of the structural components of the network (edges and nodes) visualization are fixed, the next step involves developing the quantitative metrics associated with the network topology. This quantitative metrics will provide us with a framework to characterize the eye fixation strategy and subsequently the cognitive decision making strategy of the ATC. There a mainly three node level centrality metrics considered in this manuscript namely, *Indegree*, *Closeness* and *Betweenness*. All these above mentioned centrality metrics measures

how central (in other words important) a particular node is in the overall network topology. Higher the centrality metrics value indicated higher importance. Each of the three above mentioned centrality metrics measure centrality of a node from different functionality perspective. The details about the metrics and their calculation has been described in the subsequent sections.

3.4.2.1 Indegree centrality

Indegree centrality metric – Degree or degree centrality of a node has been traditionally defined as the number of direct connection a particular node has in the network (Freeman, 1978). For undirected networks we have only one degree measure of a node which is the number of edges connected to that node. Things get different when we have directed networks where we have two measures of degree namely, indegree (indegree centrality) and outdegree (out degree centrality). Indegree and outdegree in this case is the amount of incoming edges and the number of outgoing edges respectively from the node. Things get more complex in case of directed weighted network. In this case, apart from having directed edges we also have weights associated with the edges. Thus in such scenarios the indegree centrality for a given node in defined as the amount of incoming weights to the nodes from all other nodes in the network (Newman , 2004; Barrat et al., 2004). Similarly, the outdegree for a node is defined as the total amount of weights going out from the node to all other nodes in the network. In our case, the edge weights are the number of eye fixations in that direction, since we know that the amount of eye fixation going inside an AOI is same as the amount of eye fixations going out

of that AOI (unless the AOI is either the starting or the ending AOI in the given AOI fixation sequence), we have indegree equal to outdegree.

For calculating the indegree in case of directed weighted network traditionally the following equation has been used (Newman, 2004; Opsahl, 2009):

$$\text{Indegree} = \mathrm{C_I}(i) = \sum_{\substack{j=1 \\ j \neq i}}^{N} w_{ji} \quad \ldots (3)$$

Where, w_{ji} is the weight of the edge from node "j" to node "i".

Since the sequence developed is a collapsed version of the raw fixations therefore, $j \neq i$. In other words, no self-loops are allowed in the DWN representation. Equation 3 suffers from the limitation that this measure only considers the weight of the edges (also called node strength) and it doesn't take into account the number of edges. As argued by Opsahl et. al. (2010) that the original definition of the indegree metric by Freeman (1978) considered the number of ties a node has in the network, whereas the measure generally used for weighted directed networks only considers the weights associated with the node but not the number of edges. From figure 11 we can see that for the same value of incoming weights for a particular node we can have various possible incoming edge combinations in the network topology. Therefore, there is need to consider a different degree centrality measure for directed weighted networks. Opsahl et al., (2010) provides a generalized degree centrality formula which takes into account both the weights and the number of edges, which is as follows:

$$C_I(i) = k_i \times \left(\frac{s_i}{k_i} \right)^{\alpha} = k_i^{1-\alpha} \times s_i^{\alpha} \quad \ldots (4)$$

Where,

$$k_i = \sum_{j=1}^{N} x_{ji}, \; x_{ji} = \begin{cases} 1 & \text{edge exits between node j to i} \\ 0 & \text{otherwise} \end{cases} \quad \ldots (5)$$

$$s_i = \sum_{\substack{j=1 \\ j \neq i}}^{N} w_{ji} \quad \ldots (6)$$

In the above formula "α" is the tuning parameter whose value ranges from 0 to 1. The value of α determines the relative importance given to the edge weights and the edge numbers while calculating the degree centrality value. For the present study for simplicity sake we have used α=1. As a result, the value obtained from equations 3 and 4 are same; although in future different values of α can also be considered for different applications of the obtained results depending the context.

For α=1, we have $C_I(i) = k_i^{1-\alpha} \times s_i^{\alpha} = s_i$. For demonstration purpose Consider a sample AOI fixation sequence "**ABACACADACDCDCAB"** (for simplicity sake we have not considered an overlapping case). The corresponding DWN representation of the sequence is shown in figure 12. For example, for node "A" we have an edge with weight value one coming from "B", edge with weight three coming from "C" and edge with weight one coming from "D"; therefore $C_I(A) = s_i = 2+3+1 = 6$. Thus applying the generalized formula shown in

equation 4 (for α =1) for the network shown in figure 12 we get the following indegree values for the nodes (Table 6).

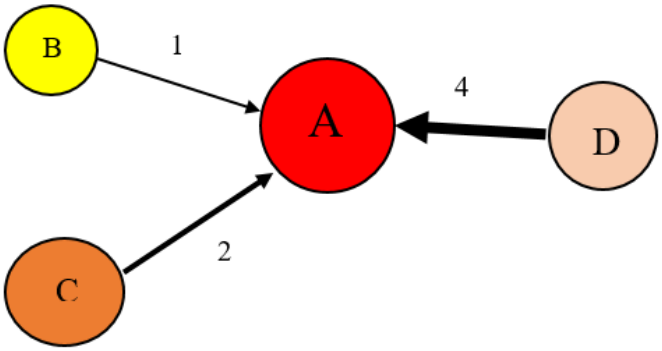

(a)

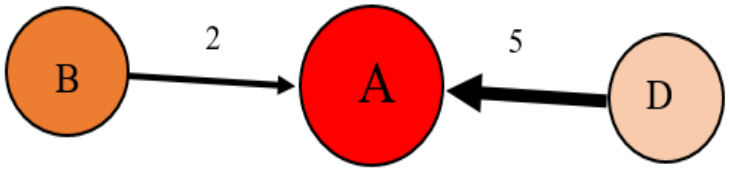

(b)

Figure 11: Example of different edge combination for the incoming weight for a node (a) node A has indegree centrality 7 and 3 incoming edges (b) node A has indegree centrality 7 and 2 incoming edges

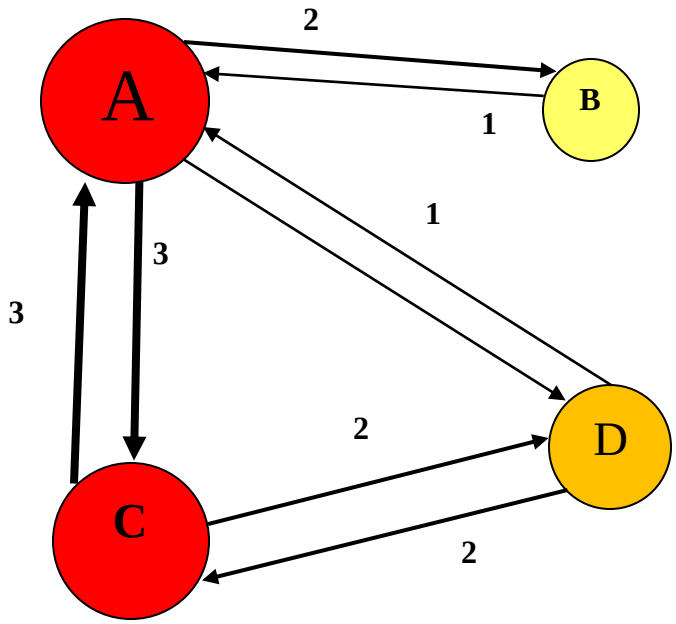

Figure 12: DWN representation of the example sequence

Table 6: Indegree values for the nodes of the network shown in figure **12** for $\alpha=1$

Node Name	Indegree
A	5
B	**1**
C	5
D	3

3.4.2.1 Closeness centrality

Closeness centrality metric: As we have seen that the indegree centrality only measures the number of direct connection a node has in the network but it doesn't talk about how on average it impacts the other nodes or how close it is to all other nodes on average. The closer a node is to all other nodes in the network,

the more importance it holds in the overall network topology and subsequently in the underlying cognitive strategy of the ATC. In the present study, we can have an AOI which have very high transition from a single AOI but not directly sharing any connection to other AOIs. As a result, for such a node it will have very high indegree value but it might not be very impactful to the overall network topology (thus overall cognitive strategy of the ATC) because it is isolated from all other nodes in the network. Thus we can see that only indegree centrality is not sufficient to measure the importance of the node in the network obtained. Thus we need to have a metric which measure how close a node is to all other nodes, in other words how reachable are all the other nodes from the particular node under consideration. This closeness or reachability of a node is measured by closeness centrality metric. The node level closeness centrality for a particular node is defined as the inverse of the sum of its minimum distances from all other nodes in the network (Freeman, 1978). Mathematically it is defined as follows:

$$Closeness = C_C(i) = \frac{1}{\sum_{j=1}^{N} d_{\min}(i, j)} \quad \ldots (7)$$

Where,

$\sum_{j=1}^{N} d_{\min}(i, j)$ is the sum of the minimum distances from node "i" to node "j" and

$j \in (1,2...N)$

Therefore, to find the minimum distance between two nodes first we need to define the concept of distance in a directed weighted network. If the edge weight in a directed graph is considered as the "cost" or the "resistance" to transverse that edge in that given direction the distance is equal to the edge weight; but if the edge weight represents the strength of the tie, then the distance in that direction can be considered as the inverse of the weight of the edge (Opsahl et. al., 2008). In the present case, the edge weight from node "i" to node "j" is equal to the number of eye fixation transitions from AOI "i" to AOI "j". Therefore, the edge weight is a representation of the strength of the tie in the direction AOI "i" to AOI "j", thus the distance from AOI "i" to AOI "j" is inverse of this weight. Mathematically, the distance from AOI "i" to AOI "j" can be written as follows:

$$d(i,j) = \frac{1}{w_{ij}} \quad \ldots (8)$$

Where, w_{ij} is the edge weight from node "i" to node "j".

For the present study the networks under consideration are directed in nature, therefore the distance from node "i" to node "j" is different from node the distance from node "j" to node "I".

In case of directed network data, it is often noticed that sometime there is no direct edge connecting two nodes, e.g. in figure 12 we cannot travel directly from node "B" to node "D", but we need to traverse either from "B" to "A" then to "D" or either from "B" to "A" to "C" and then to "D". In such cases the minimum

distance needs to calculated by taking into account the distance to all the intermediate nodes in the possible shortest route (which depends on the edge weights). Mathematically it can be shown as follows (Opsahl, et. al., 2010):

$$d_{\min}(i, j) = \left(\frac{1}{w_{ik_1}} + \frac{1}{w_{k_1k_2}} + \ldots + \frac{1}{w_{k_nj}} \right) \quad \ldots (9)$$

Where,

$k_1, k_2 \ldots k_n$ are the intermediate nodes that needs to be crossed while travelling from node "i" to node "j".

$w_{k_mk_n}$ is the weight of the edge joining the nodes "k_m" and "k_n"

While calculating the shortest distance between nodes another very important point that needs to be taken into account is that for the present case the edge weights are representation of the strength of the ties between the nodes in that direction. As a result, higher the weight for a particular edge, lower is the distance between the nodes in that particular direction (equation 9). Thus, there can be many instances where the direct edge connecting two nodes may not be the shortest route between those two nodes, whereas an indirect route having intermediate nodes may turn out to be the shortest possible route. Figure 13 shows such an example, where the shortest route between node "A" to node "D" is not the direct edge having weight 1 but the route from node "A" to node "C" and then to node "D" (shown by the blue direction line).

Using equation 8 and 9, we get

$$d(A,D) = \frac{1}{w_{AD}} = 1 \text{ and } d(A,C) + d(C,D) = \frac{1}{w_{AC}} + \frac{1}{w_{CD}} = \frac{1}{3} + \frac{1}{2} = \frac{5}{6}$$

Thus, we get $d(A,C) + d(C,D) < d(A,D)$

Using equation 8 and 9, and taking note of the above mentioned point we get the following table that shows the distance between nodes in the sample network shown in figure 12.

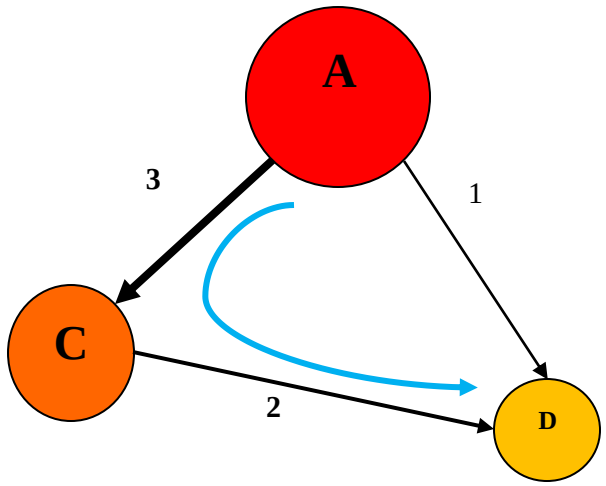

Figure 13: Example of shortest distance between two nodes. The shortest path from node "A" towards node "D" is shown using the blue curve.

Table 7: Minimum distance matrix of the sample network shown in figure 12

From node	To node			
	A	**B**	**C**	**D**
A	0.00	0.50	0.33	0.83
B	1.00	0.00	1.33	1.83
C	0.33	0.83	0.00	0.50
D	0.83	1.33	0.50	0.00

From table 7 we get that the average distance between the nodes is 0.845 (which is the average of the entries in table 7, neglecting the diagonal entries). We should note that it is difficult to define the physical interpretation of the average distance value thus obtained. To solve this issue Opsahl et al.,(2010) advocates the normalization of the weights of the given network by the average weight of the network. This normalization is to be done before calculating the distance between the nodes. Mathematically it is defined as follows:

$$w_{ij,norm} = \frac{w_{ij}}{w_{avg}} \quad \ldots (10)$$

$$w_{avg} = \frac{\sum_{i=1}^{N}\sum_{\substack{j=1 \\ i \neq j}}^{N} w_{ij}}{N(N-1)} \quad \ldots (11)$$

Since, we are not taking into account the diagonal elements of the distance matrix therefore the denominator in equation 10 is N(N-1) = 4*(4-1) =12. For the

figure 12 the average weight is 1.25. After normalizing the weights, we obtained the following network shown in figure 14. After the weight normalization the subsequent distance matrix obtained is shown in table 8. Thus, the distance obtained after the normalized weights can used can be represented as follows;

$$d_{ij,norm} = \frac{1}{w_{ij,norm}} = \frac{w_{avg}}{w_{ij}} = k \times w_{avg} \quad \ldots (12)$$

Where, $k = \frac{1}{w_{ij,norm}}$

From equation 12 we can see that the normalized distance between node "i" to node "j" can be interpreted as a scalar multiple of the average weight of the network. Now the normalized average distance among the nodes is equal to 1.058; which can be interpreted as 1.058 times the average weight of the network (Opsahl et al., 2010). After the distances have been calculated now we can proceed towards the calculation of the closeness value of the nodes in the network. For example, the closeness values for node "A" is as follows:

$$Closeness\ of\ node\ A = C_C(A) = \frac{1}{0.625 + 0.42 + 1.04} \approx 0.48$$

Table 9 shows the closeness values for all the nodes of the network shown in figure 14.

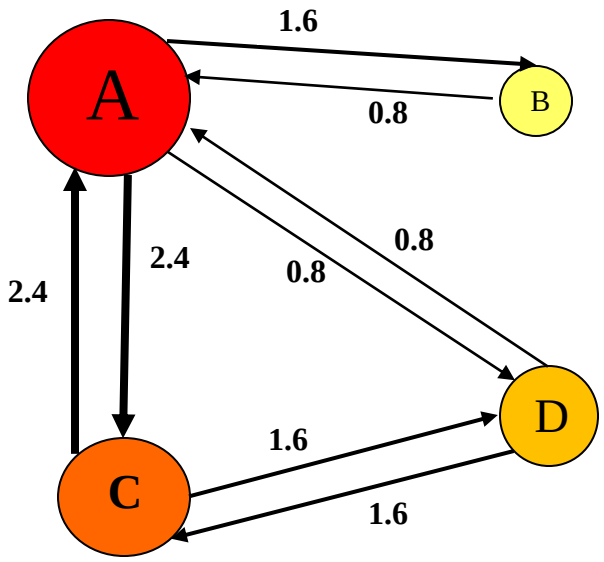

Figure 14: DNW representation of the sample sequence after weight normalization

Table 8: Distance between nodes after weights are normalized for the network shown in figure 14

From node	To node			
	A	**B**	**C**	**D**
A	-	0.63	0.42	1.04
B	1.25	-	1.67	2.29
C	0.42	1.04	-	0.63
D	1.04	1.67	0.63	-

Table 9: Closeness metric value for nodes of the network shown in figure 14

Node name	Closeness
A	0.480
B	0.192
C	0.480
D	0.300

3.4.2.1 Betweenness centrality

Betweenness centrality metric: The above mentioned two centrality metrics namely, indegree and closeness measure the importance of a node by measuring the direct association of the node and how much it is reachable to all other nodes in the network respectively. As a result, nodes having very high amount of direct association with other nodes and nodes having very high reachability to other nodes will have high indegree and closeness value respectively; although we encounter some instances where a node which doesn't have either of the above discussed properties but still plays an important role in the network dynamics just by being present on the critical path connecting two dis-connected group of nodes (figure 15). Because of this presence, every information transaction that happens between these two disjoint group of nodes passes through the specific node which connects these two group of nodes. As a result, this specific node becomes important from information transaction/ flow point of view. This importance of a node from the information transaction context point of view is captured by the betweenness centrality metric.

In a given network, betweenness for an arbitrary node "i" is defined as the ratio of number of shortest path between any two random nodes passing through node "i" to the number of shortest path between those two random nodes concerned. Let g_{jk} is the total number of shortest path between node "j" to "k" and the let $g_{jk}(i)$ be the number of those shortest path between node "j" to "k" that passes through node "i"; then the betweenness metric value of the node "i" is defined as ratio of

$g_{jk}(i)$ over g_{jk} summing over all possible combination of node "j" and node "k" in the network. Mathematically this can be written as follows (Opsahl et al., 2010):

$$Betweenness = C_B(i) = \sum_{j \neq k \neq i} \frac{g_{jk}(i)}{g_{jk}} \quad \ldots (13)$$

Where,

$\sum$ represents summed over all possible combination of index "j" and index "k"

For an example case lets calculate the betweenness value for node "A" for the sample network in figure 12. Table 10 represents all possible combination of starting and ending nodes for which the shortest paths needs to be calculated w.r.t the network topology shown in figure 12. From the figure we can see that shortest route between node "B" to node "C", node "B" to node "D", node "C" to node "B", node "D" to node "B" all pass through node "A". The other two combinations that doesn't have node "A" as either the starting or the ending nodes are path from node "C" to node "D" and node "D" to node "C" and for these two combinations their shortest route doesn't pass through node "A". Therefore, using equation 13 and possible pair combination from table 10 we get the following values for node "A":

$$\frac{g_{BC}(A)}{g_{BC}} = \frac{1}{1}, \frac{g_{BD}(A)}{g_{BD}} = \frac{1}{1}, \frac{g_{CB}(A)}{g_{CB}} = \frac{1}{1}, \frac{g_{DB}(A)}{g_{DB}} = \frac{1}{1}$$

Therefore, from equation 13 we get,

$$C_B(A) = \frac{g_{BC}(A)}{g_{BC}} + \frac{g_{BD}(A)}{g_{BD}} + \frac{g_{CB}(A)}{g_{CB}} + \frac{g_{DB}(A)}{g_{DB}} = 1+1+1+1 = 4$$

Table 11 represents the betweenness scores of all the nodes of the sample network shown in figure 12.

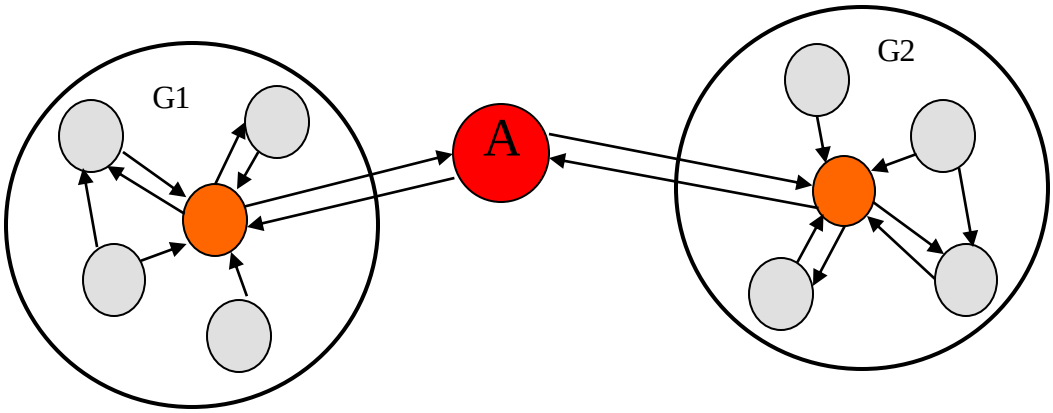

Figure 15: Example of a node lying on the critical path joining two otherwise dis-connected node groups. Node "A" is only connected to two important nodes belonging to group1 and group2 (shown in orange colour), as a result it lies on the critical path between the two groups.

Table 10: All possible combination of starting and ending nodes for which the shortest paths needs to be calculated for the network in figure 12

From	To	From	To
A	B	C	A
A	C	C	B
A	D	C	D
B	A	D	A
B	C	D	B
B	D	D	C

Table 11: Betweenness value of the nodes of the network shown in figure 12

Node name	Betweenness
A	4
B	0
C	4
D	0

Chapter 4: Results

This section describes the results obtained from the analysis of the data collected from the experiment performed at the FAA CAMI in OKC. The information presented in this section has already being published in Mandal, et. al., (2016). For demonstration purpose of the proposed algorithm the analysis of only one ATC's eye tracking data has been provided as a pilot study.

As mentioned in section titled "simulation experiment", we know that the total experimental scenario duration was of 20 minutes. For analysis purpose the total duration was divided into 4 equal parts of 5 minutes each. A detailed analysis of the first five-minute duration (starting from 0 minute and ending at 5 minute) has been explained in detail in the following section. A comparative analysis of the results obtained for this 5 minute duration and the total 20 minute has been done subsequently.

4.1 Results: 0-5 minute duration

Table 12 shows the various aircraft present in the 0-5 minutes' duration and their respective AOI character names used for the analysis purpose. Table 13 shows a small sample of the AOI fixation sequence obtained for this duration of the simulation scenario. The total cumulative eye fixation duration that happened on the various AOI combination during this duration is shown in figure 16. From the figure 16 we can see that highest duration of eye fixation occurred on AOI "H". AOI "A", "G" and "F" also received substantial eye fixation duration approximately in the range of 11-13 seconds. The next in the line is the AOI "E"

which is fixated upon for around 9 seconds approx. Another important aspect to notice from the plot is that the eye fixation duration on the overlapped AOI states (e.g. “A,B”, “B,E” etc.) is very small in value. The possible reason for this might that the overlapping states occur for very short duration of time, as a result the ATC spends very short amount of time on these states. Unlike this, one overlapping AOI state named “H,I” have substantial eye fixation duration attributed to it. This result can be understood from the fact that one of the participating individual AOI states “H” in the overlapping state “H,I” has very large amount of eye fixation duration associated with it. Thus, it might be possible that the ATC controller was actually fixating upon on the AOI “H” but due to overlapping with AOI “I” the algorithm mapped those eye fixations and subsequently the fixation duration with the overlapped AOI state.

Table 12: Aircraft's name and their corresponding AOI name. Table adapted from Mandal et al., (2016).

Aircraft Name	AOI Name
AAL2892	A
AAL631	B
N421TA	E
SWA234	F
SWA3698	G
AWE7523	H
DAL3618	I
FDX3621	J

Table 13: Sample AOI fixation sequence for 0-5 minute duration

In/out flag	Eye fix. Index	# of eye fix.	AOI name list	Eye fix. time duration (secs.)
1	1	1	A	0.2
0	[2,3,4]	3	-1	1.2
1	5	1	[H,I]	0.8
1	[6,7]	2	G	0.5

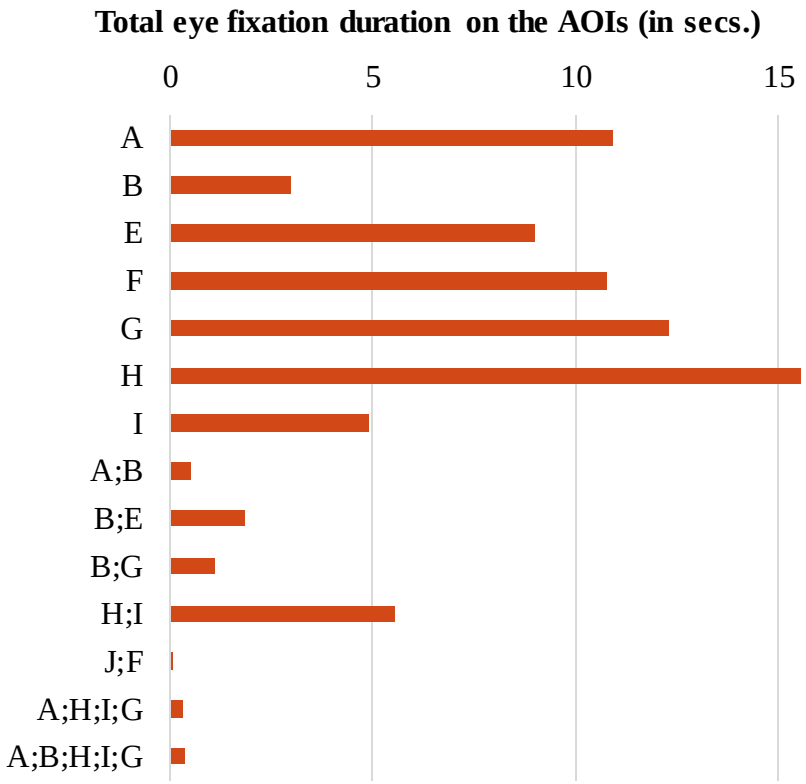

Figure 16: Total cumulative eye fixation time on various AOIs for 0-5 minute duration. *Figure adapted from Mandal et al., (2016).*

Figure 17 shows the DWN visualization of the AOI fixation sequence for 0-5 minute time segment of the simulation scenario. From the figure we can see that the most important AOI w.r.t the size of the node is AOI "A", "G" and "I". As far as the colour attribute of the nodes are concerned the AOI "A", "G" and "H" are the most important. This information is also substantiated from the figure 16. For the case of AOI "I" it has large size but a more yellowish colour to it, signifying that the large number of eye fixation fixated upon it are of small duration only. The small size and the red colour of the AOI "F" can be understood by the fact that the ATC has made few number fixations on AOI "F" but each fixations had long duration associated with it. AOI "E" has substantial eye fixation number and duration associated with it as evident from the slightly reddish colour and size of the node. As expected, all the overlapped AOI states are both small in size and yellow in colour, except AOI "H,I" whose reasoning has been explained above.

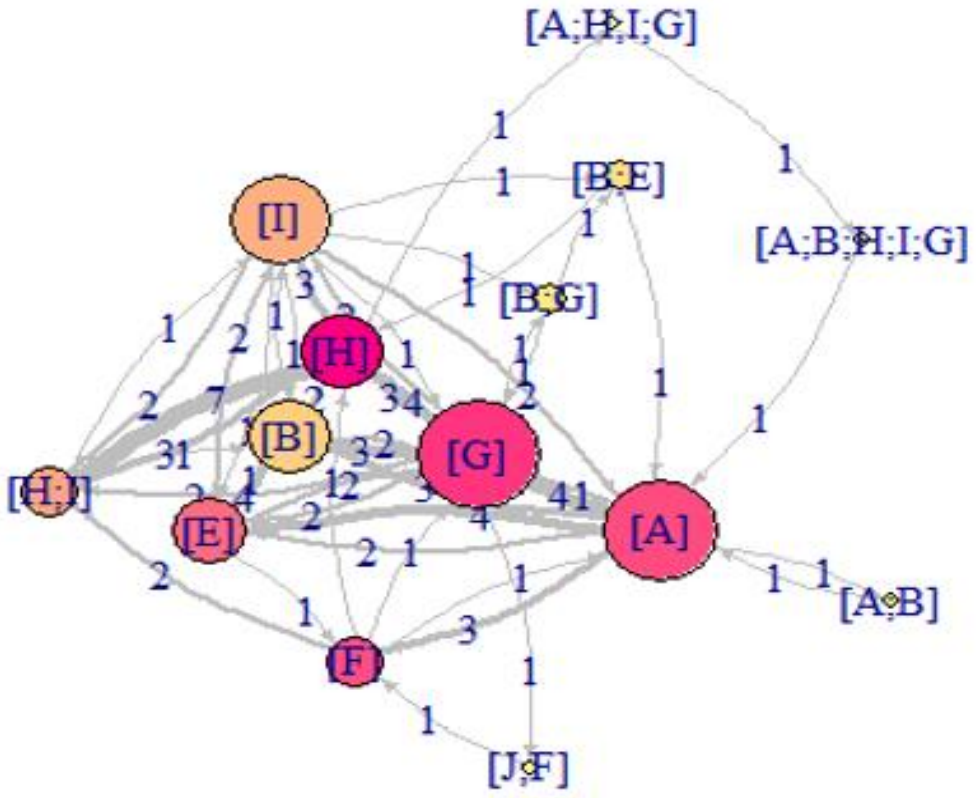

Figure 17: DWN visualization of the AOI fixation sequence data for 0-5 minute duration. *Figure adapted from Mandal et al., (2016).*

Figure xx represents the indegree centrality metric values for the various AOI states present in the 0-5 minute duration. As expected from the DWN visualization in figure 17, the indegree plot (figure 18) also shows that the most important AOIs are "A", "G" and "H". The next set of AOI which have substantial amount of eye fixations (as represented by the indegree value) are states namely, "B", "E", "I" and the overlapped AOI state "H,I".

The closeness and betweenness centrality metrics are shown in figure 19 and 20 respectively. Form the figure 19 we can see that the closeness metric also follows a similar profile like indegree metric value. This plot shows that AOI "A", "G" and "H" are closer to all other nodes in the network compared to other given AOI states in the DWN visualization. This fact can be confirmed from the fact that most of the eye fixation transition from all other nodes happens to these nodes, as shown by the node large node size of these AOIs in the DWN visualization in figure 17.

Unlike closeness and indegree metric results, the plot for the betweenness metric value (which represents how important role a given node plays in the transmission of information, eye fixation transition in our case, between any two random nodes in the network) shows some interesting results. Aircraft "A" has distinct large value of betweenness compared to other aircraft; which shows that it plays an important role while the ATC makes transition from one aircraft towards another. In other words, aircraft "A" plays as an information hub through which the information exchange, eye fixation transition in our case, between various aircraft happens. As expected all the overlapped AOI states have very low betweenness value. Aircraft "G" and "H" have similar betweenness centrality value of approx. 50. Thus, the betweenness metric values shows that in the overall scanning strategy of the ATC, the aircraft "A", "G" and "H" plays very vital role as most of the shortest routes connecting various aircrafts passes mostly through these three aircrafts.

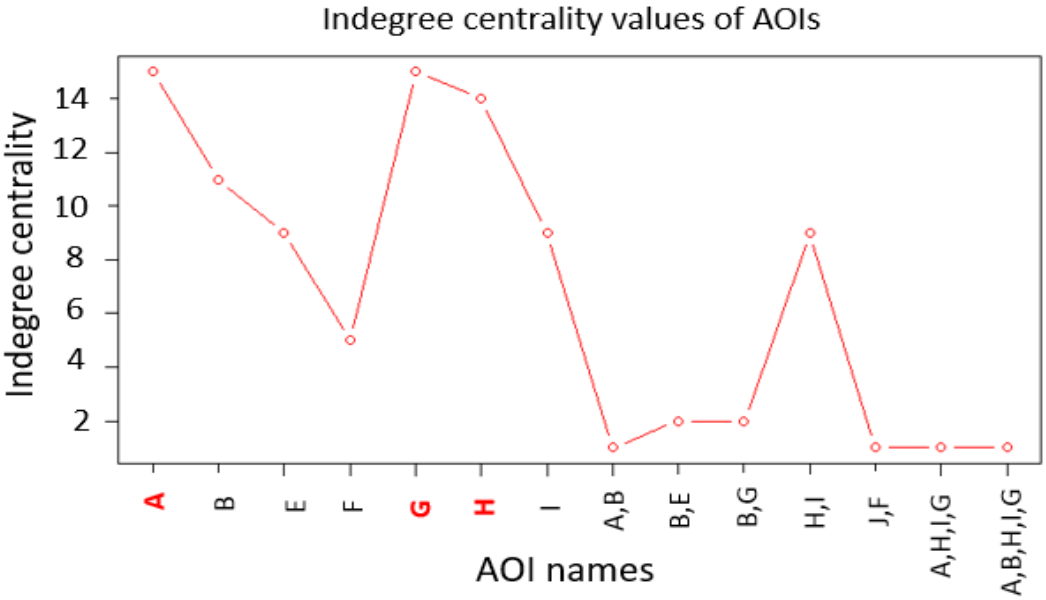

Figure 18: Indegree centrality metric value for various AOIs for 0-5 minute duration. *Figure adapted from Mandal et al., (2016).*

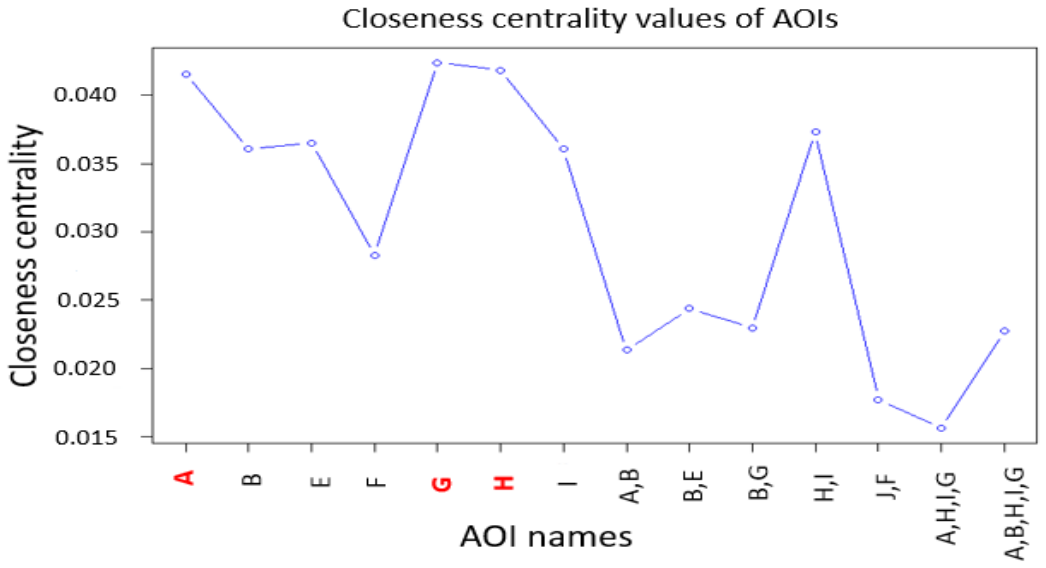

Figure 19: Closeness centrality metric value for various AOIs for 0-5 minute duration. *Figure adapted from Mandal et al., (2016).*

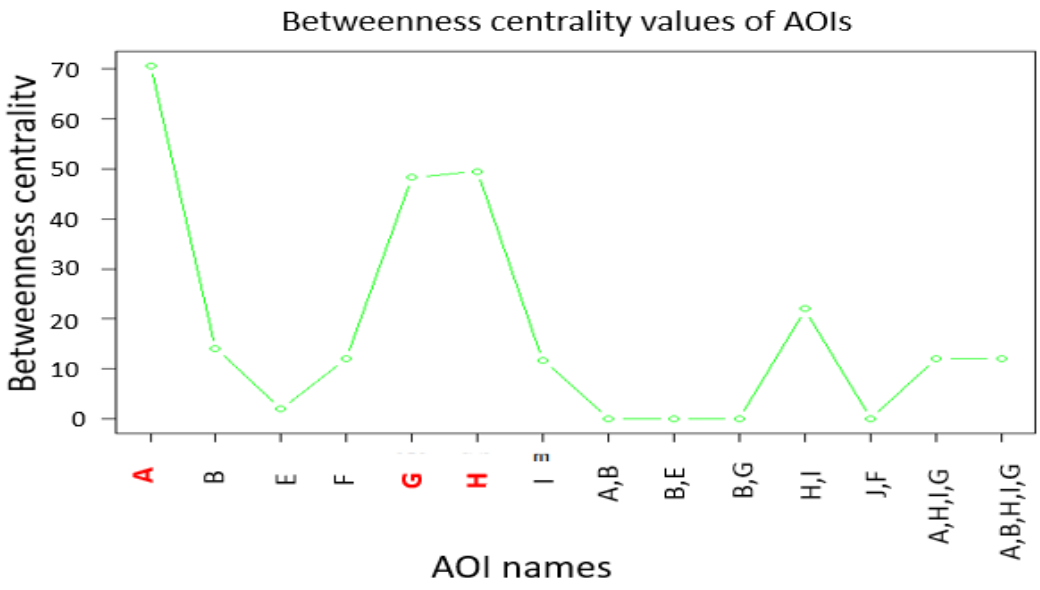

Figure 20: Betweenness centrality metric value for various AOIs for 0-5 minute duration. *Figure adapted from Mandal et al., (2016).*

To understand the particular characteristic obtained in the DWN visualization and the centrality metric plots for the 0-5 minute duration of the scenario we need to carefully investigate the video recording for the same. Figure 21 represents the snapshot of the video of the scenario for the 4th minute of the scenario under consideration. The figure shows the AOI names and also the direction in which the respective aircraft are moving. Three larger regions of interest in the snapshot are shown in red, blue and green boundaries. In the red region we can see that the aircraft with AOI name "A" and "G" are moving head-on. Due to this a possible conflict situation may arise; as a result, the ATC has spent substantial amount of eye fixation duration on these two AOIs (as evident from

figure 16) and has made many transition movements between these two AOIs (as evident from the thick edge joining node A and G in figure 17).

Another important region is the region in green boundary where aircraft with AOI name "H" and "I" are present. On careful investigation of the recorded video it is noticed that the aircraft "H" makes a direction change around the 4th minute and starts moving towards the line joining aircraft "A" and "G". As a result, the ATC spend substantial amount of time to investigate any possible future conflict situation. Another important thing is that aircraft "H" and "I" are moving one after the other with very high physical proximity with each other on the display; although this doesn't give to any possible conflict situation due to difference in their flying altitude. These above two reasons must have contributed to that fact that aircraft "H" has high amount of eye fixation duration attributed to it. The unlikely increase in the eye fixation duration associated with the overlapped AOI state "H,I", unlike other overlapped states, is mainly because of the contribution from the importance held by AOI "H".

The last major region to focus is shown in blue boundary. This region has aircraft with AOI names "A", "B" and "E". As we can see from the figure 21 that all these three aircraft are in close physical proximity w.r.t each other. Aircraft "A" and "B" are crossing each other although there is a huge altitude difference in them. As a result, there doesn't arise any possible future conflict scenario among them. Once aircraft "B" moves past aircraft "A" there is no other aircraft in front of it, thus once the ATC is confirmed that there is no possible conflict between "A" and

"B" he/she cease to pay much attention to it, resulting in low eye fixation duration on "B". Unlike this aircraft "E" is approaching towards "A" as visible form the 4th minute snapshot shown in figure 21. Apart from that during the time interval after the 4th minute, the trajectory of aircraft "E" crosses the trajectory of many other aircrafts such as "G", "H and "I". As a result, the ATC is subjected to divert his attention toward aircraft "E" which results in it having substantial eye fixation duration associated with (figure 16 and 17).

Another important fact noticeable from the figure 17 is that aircraft F has very small node size unlike the other red coloured nodes in the network. A possible reason can be found after investigating the snapshot figure 21 where we can see that at the 4th minute the aircraft "F" has just entered the visual display and its speed vector is not yet displayed. As a result, after preliminary investigation of the information provided in the data block of the aircraft "F" for a certain amount of time the ATC doesn't visit it anymore resulting into high eye fixation duration but low number of fixations associated with it. The low number of eye fixation transitions to the aircraft "F" from all other aircraft can be understood by the fact that it has very large lateral distance from other aircraft on the display.

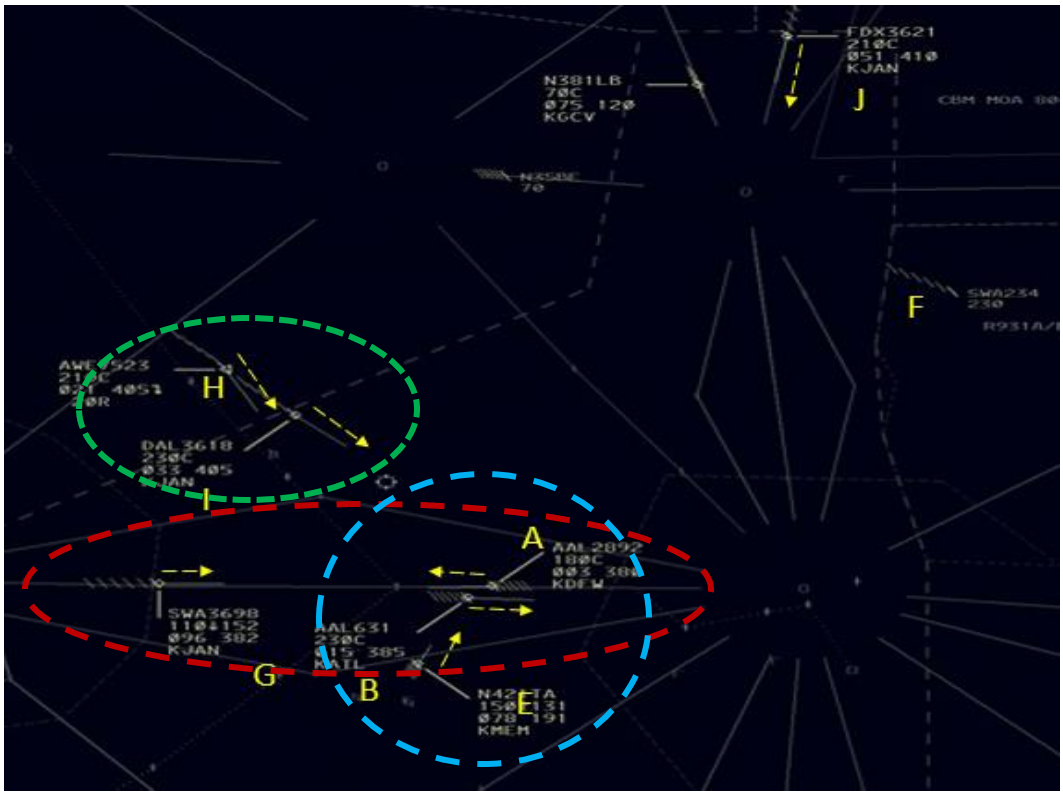

Figure 21: Snapshot of the simulation scenario at 4th minute. *Figure adapted from Mandal et al., (2016).*

4.2 Results: 0-20 minute duration

Figure 22 represents the DWN visualization of the total 20 minutes duration of the simulation scenario under consideration. As we can see from the figure that the network has grown very complex in nature with many new nodes and as a result many new edges appearing. The nodes which have substantial number of fixations associated with them have been named for the ease of visualization purpose. For the similar reason the edge weights are also are not shown in the figure.

The most important fact visible from the figure 22 is that for the whole 20-minute duration the important aircraft, w.r.t node size and node colour, are different as compared to the previous 0-5minute duration DWN visualization. The most important aircraft for the whole 20 minutes duration are aircraft "E", "H" and "I". On careful investigation of the recorded video of the scenario, it is noticed that aircraft "A" leaves the visible display at the 8^{th} minute and similarly, aircraft "G" descends down to the airport at around the 14^{th} minute. This is the reason why the two previously important aircraft ceases to hold crucial position in the overall scanning strategy of the ATC for the whole 20 minutes duration. Unlike these two aircrafts the aircraft "E", "H" and "I" remains visible on the display area for the whole of 20 minutes duration, which explains why they become more important for the eye fixation strategy of the ATC.

The new nodes appearing in the figure 22 can be explained by the fact that with passage of time many new aircraft appear on the display area, as a result giving rise to many new singular and also many overlapping AOI states which was previously not there for the 0-5 minute duration. Table 14 shows the cumulative eye fixation duration and also the various centrality metric values for the three most important aircraft for the 0-20 minute duration.

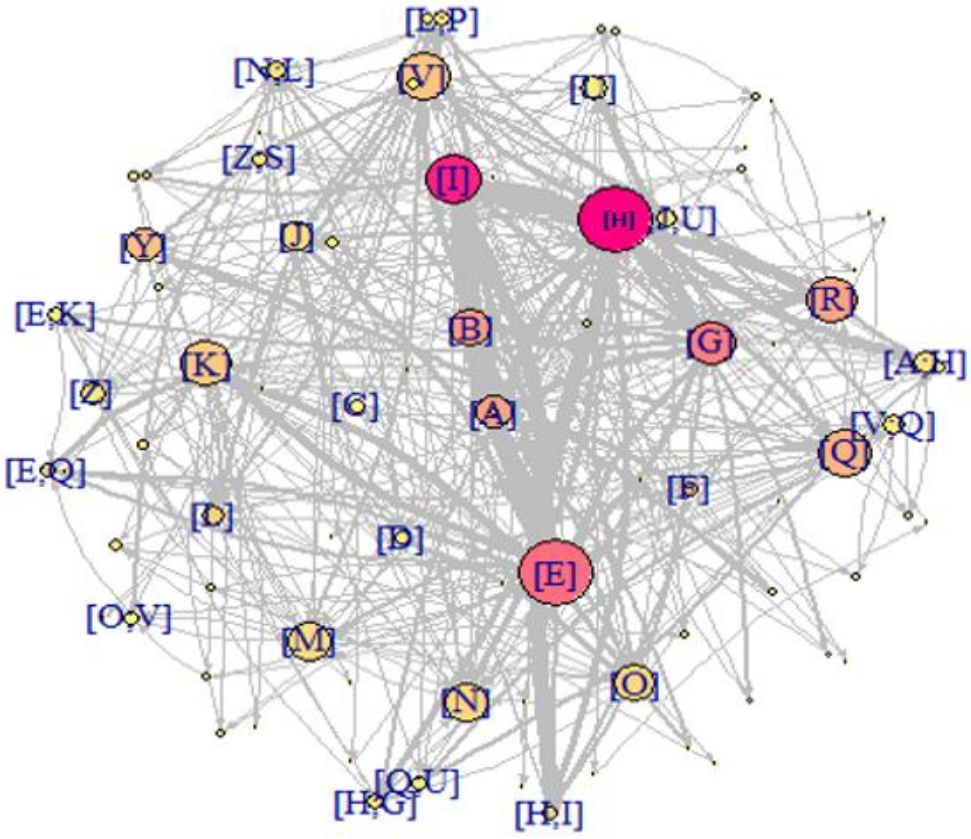

Figure 22: DWN visualization of the AOI fixation sequence data for 0-20 minute duration. *Figure adapted from Mandal et al., (2016)*

Table 14: Centrality metric values for the 3 most important aircraft for 0-20 minute duration. *Table adapted from Mandal et al., (2016)*

AOI	Total eye fixation time (s)	Centrality metrics		
		Indegree	Closeness	Betweenness
E	19.485	33	0.0053	1810
H	34.045	41	0.0054	2373
I	29.614	31	0.0053	1240

Chapter 5: Discussions & Conclusion

5.1 Discussions

The prevalent eye fixation visualization techniques of can be classified into two main categories namely, point based and AOI based. The visualization techniques, in both the categories mainly deal with static scenarios or scenarios having static AOI locations. The other major limitation is that they are not equipped to handle scenarios where the number of AOI are changing with time. It is also very difficult to develop advanced quantitative metrics from these techniques, as a result they are not very efficient in scenarios where the objective is to understand complex eye tracking strategies and subsequently the underlying cognitive process of the onlooker.

For the present study, the scenario under consideration was dynamic in nature, i.e. the aircraft were moving on the display. Apart from that, the number of aircraft were also changing with time. Given this scenario, our main objective is to understand the eye fixation strategy of the ATC. Due the above mentioned specific characters of the scenario under consideration the prevalent techniques don't serve the intended objective very efficiently. Therefore, it is necessary to develop a new visualization methodology with can address these major limitation, i.e. which can handle dynamic AOIs, change in the number of AOIs and also is suitable enough for the development of advanced quantitative metrics.

The present paper demonstrates the development of a new visualization technique using the directed weighted network (DWN) approach. In the network

the nodes/ vertices represent the AOI of the aircraft's, and the edges (which are directed and weighted) represents the eye fixation transition in a particular direction. The weight of the edges represents the amount of eye fixation transition that occurred in that direction. Apart from that, few visual attributes of the network structure have also been employed to make the visualization process more intuitive. The size of the node has been made proportional to the amount of eye fixation happening on that particular node/ AOI. The colour of the node also depends on the amount of cumulative eye fixation time spent on the it. Higher the eye fixation duration more reddish in the colour of the node, and lower the amount of eye fixation time more yellowish is the colour of the node. The thickness of the edge is proportional to the weight of the edge.

Thus we can see that with the application of the DWN representation enables us to visually represent the characteristics of eye fixations, such as number of fixations and their cumulative duration on each of the AOIs. Application of the visual attributes in the DNW representation lets us visually inspect which AOIs were more important than others (viewed more often than others) and also which are the AOIs among which very high amount of eye fixation transitions have happened. Apart from the visual attributes, the DNW visualization also helps us to in the development of advanced quantitative metrics (indegree, closeness, and betweenness centrality measures) which provides a quantitative framework to understand the relative importance of the AOIs in the overall fixation strategy of the onlooker. The framework thus provides a quantitative means to investigate the

underlying cognitive processes that formed such different networks topologies. The ability of extracting the quantitative framework from the DNW representation makes it a viable candidate towards the development of a methodology for comparisons of various eye fixation strategies also. The DWN methodology also has the ability to address issues of dynamicity of the AOIs in terms of disconnected graphs or stochastic graphs. Therefore, this methodology can be further developed for addressing the issue of the spatio-temporal aspects of the eye fixation data.

One important thing about the results obtained is that the important AOIs, in the eye fixation strategy, changes with change in the time segment used for analysis. This fact is visible from the results obtained for the 0-5 minute duration in comparison to the 0-20 minute duration of analysis. This difference of results obtained for different time segments shows that we also need to develop a guiding mechanism to determine the optimal time segments for analysis purpose.

5.2 Conclusion

The traditional methods of eye fixation visualization are not efficient to handle scenarios which have the dynamic AOIs and also whose numbers are changing with time. They also lack the development of advanced quantitative metrics to analysis complex eye fixation strategies. Therefore, to address these limitations we have proposed a new methodology of using DWN visualization. This new visualization approach can effectively represent the important AOIs in the fixation strategy being employed, using only visual attributes. Many other attributes of the eye fixation data, e.g. eye fixation numbers, eye-fixation duration on

AOIs and direction of transitions, can also be represented using this framework. The proposed new method also provides a framework for the development of advanced quantitative metrics for the analysis of complex eye movement data. The quantitate metrics can be used to compare between two eye fixation strategies. It is also noticed that the results obtained from the proposed methods is very much dependent on the time segment used for the analysis purpose because of the dynamic nature of the scenario considered for the experiment. Thus, we need to consider a guided mechanism to determine an optimal strategy to perform this time segment selection.

Chapter 6: Limitations & Future Work

6.1 Limitations

Given the present form of the DWN algorithmic, one major limitation observed is that the results are every much effected by the time segment we choose for the analysis purpose. With change in the start and ending time of the analysis time segment the subsequently obtained values of the important aircraft in the AOI fixation sequence also change. Thus, an absence of a guided method to segment the time duration for analysis purpose is presently missing.

Another major noticeable limitation of the DWN visualization process is that, given the network data it is not possible to extract the unique AOI fixation sequence from which the given network is developed from. Thus, the mapping function from the AOI fixation sequence set to the network visualization data set doesn't have any inverse, since the reverse mapping doesn't generate any unique AOI fixation sequence.

We need to understand the fact that the given form of the DWN visualization is an abstract and a static form of representing the AOI fixation sequence which have both spatial and temporal attributes attached to it. Since we are using a static approach to visualize the AOI fixation sequence data, where the AOIs are changing their position and shape with time, it is not possible to represent the actual trajectories of the AOIs. DWN approach, being a static representation, also limits the possibility of representing the actual spatial distribution of the eye

fixation data. Although, the major objective being understanding the AOI fixation strategy the above mention limitation doesn't have much adverse impact on the results obtained from the DWN approach.

6.2 Future work

As a part of the future work, we can consider addressing some of the above mentioned limitations of the present form of the proposed algorithm. For the present study, because of the dynamic nature of the simulation scenario new aircraft (as result the corresponding AOIs) can enter the display and already present aircraft can leave the display area with passage of time. As a result, the spatial location of the aircraft and the number of them visible on the display change with time. To represent the AOI fixation data on such a scenario the concept of dynamic graphs can be applied. instead of using a single graph representing the whole scenario we can consider using several graphs representing the changing dynamics of the AOI fixation sequence with the dimension of time attached to it. Another possibility for future endeavor is to analyses the AOI fixation sequence data using a network having stochastic attributes.

Apart from the network visualization approach, we can also consider analyzing the algebraic properties of the AOI transition matrix obtained from the AOI fixation sequence data. The spectral analysis of the AOI transition matrix can help us to unearth the various inherent structural similarities or dissimilarities

existing among the various AOI fixation sequences, obtained from various ATC's eye fixation data, which are otherwise not apparent from simple visual examination of the network visualization. This method will allow us to better characterize AOI fixation sequence data for obtained from experiments of long time duration.

Another approach that can be applied for further analysis of the AOI fixation sequence data is to treat the eye fixation data as a random walk over a dynamic graph. In this case, the aircraft simulation scenario can be thought of as a completely connected dynamic graph and the eye fixation transition from one aircraft to another aircraft as a random walk process over the various nodes (aircraft) of the graph.

References

Aula, A., Majaranta, P., & Räihä, K.-J. (2005). Eye-Tracking Reveals the Personal Styles for Search Result Evaluation. In *INTERACT: IFIP International Conference on Human Computer Interaction* (pp. 1058–1061). Rome, Italy. http://doi.org/10.1007/11555261_104

Barber, C. B., Dobkin, D. P., & Huhdanpaa, H. (1996). The quickhull algorithm for convex hulls. *ACM Transactions on Mathematical Software*, *22*(4), 469–483. http://doi.org/10.1145/235815.235821

Barrat, A., Barthélemy, M., Pastor-Satorras, R., & Vespignani, A. (2004). The architecture of complex weighted networks. *Proceedings of the National Academy of Sciences of the United States of America*, *101*(11), 3747–3752. http://doi.org/10.1073/pnas.0400087101

Blascheck, T., Kurzhals, K., Raschke, M., Burch, M., Weiskopf, D., & Ertl, T. (2014). State-of-the-Art of Visualization for Eye Tracking Data. In *Eurographics Conference on Visualization (EuroVis)* (pp. 1–20). Swansea, UK.

Blignaut, P. (2010). Visual span and other parameters for the generation of heatmaps. In *Eye Tracking Research and Applications Symposium (ETRA)* (pp. 125–128). Austin, Texas, USA. http://doi.org/10.1145/1743666.1743697

Duchowski, A. T., Price, M. M., Meyer, M., & Orero, P. (2012). Aggregate gaze visualization with real-time heatmaps. In *Proceedings of the Symposium on Eye Tracking Research and Applications - ETRA '12* (Vol. 1, pp. 13–20). Santa Barbara, California. http://doi.org/10.1145/2168556.2168558

Ekstremmakina.com. (2016). "faceLab 5-SeeingMachines." Retrieved October 18, 2016, from http://www.ekstremmakina.com/EKSTREM/product/facelab/index.html

Eyetracking.com. (2016). "Powerful eye tracking software developed for researchers." Retrieved October 16, 2016, from http://www.eyetracking.com/Software/EyeWorks

Freeman, L. C. (1978). Centrality in social networks conceptual clarification. *Social Networks*, *1*(3), 215–239. http://doi.org/10.1016/0378-8733(78)90021-7

Goldberg, J. H., & Helfman, J. I. (2010). Scanpath clustering and aggregation. In *Proceedings of the 2010 Symposium on Eye-Tracking Research & Applications - ETRA '10* (pp. 227–234). Austin, Texas. http://doi.org/10.1145/1743666.1743721

Goldberg, J. H., & Kotval, X. (1999). Computer interface evaluation using eye movements : methods and constructs. *International Journal of Industrial Ergonomics*, *24*(1999), 631–645. http://doi.org/10.1016/S0169-8141(98)00068-7

Grindinger, T., Duchowski, A. T., & Sawyer, M. (2010). Group-wise Similarity and Classification of Aggregate Scanpaths. In *Eye Tracking Research & Applications (ETRA) Symposium* (pp. 101–104). Austin, Texas. http://doi.org/10.1145/1743666.1743691

Holland, C., & Komogortsev, O. V. (2011). Biometric identification via eye movement scanpaths in reading. In *International Joint Conference on Biometrics, IJCB 2011* (pp. 1–8). Washington, DC, USA. http://doi.org/10.1109/IJCB.2011.6117536

Howe, P. D. L., Drew, T., Pinto, Y., & Horowitz, T. S. (2011). Remapping attention in multiple object tracking. *Vision Research*, *51*(5), 489–495. http://doi.org/10.1016/j.visres.2011.01.001

Just, M. A., & Carpenter, P. A. (1976). Eye fixations and cognitive processes. *Cognitive Psychology*, *8*(4), 441–480. http://doi.org/10.1016/0010-0285(76)90015-3

Kang, Z., & Bass, E. J. (2014). Supporting the eye tracking analysis of multiple moving targets : Design concept and algorithm. In *Proceedings of the IEEE International Conference on Systems, Man, and Cybernetics (SMC '14)* (pp. 3184–3189). San Diego, CA, USA.

Kang, Z., & Landry, S. J. (2014). Using Scanpaths as a Learning Method for a Conflict Detection Task of Multiple Target Tracking. *Human Factors: The Journal of the Human Factors and Ergonomics Society*, *56*(6), 1150–1162. http://doi.org/10.1177/0018720814523066

Kang, Z., & Landry, S. J. (2015). An Eye Movement Analysis Algorithm for a Multielement Target Tracking Task : Hierarchical Clustering. *IEEE Transactions on Human-Machines Systems*, *45*(1), 13–24.

Kang, Z., Mandal, S., Crutchfield, J., Millan, A., Manning, C. A., & McClung, S. (2016). Designs and algorithms to map eye tracking data with dynamic multi-element moving objects. *Computational Intelligence and Neuroscience*, *2016*(1).

Kurzhals, K., Heimerl, F., & Weiskopf, D. (2014). ISeeCube : Visual Analysis of Gaze Data for Video. *Proceedings of the ETRA Conference*, 43–50.

Lankford, C. (2000). Gazetracker: software designed to facilitate eye movement analysis. *Proceedings of the Symposium on Eye Tracking Research & Applications - ETRA '00*, 51–55. http://doi.org/10.1145/355017.355025

Mandal, S., & Kang, Z. (2015). Eye Tracking Analysis Using Differently Shaped Areas of Interest to Represent Multi-Element Moving Objects. In *Proceedings of the Human Factors and Ergonomics Society 59th Annual Meeting* (pp. 1515–1519). Los Angeles, California, USA.

Mandal, S., Kang, Z., & Millan, A. (2016). Data Visualization of Complex Eye Movements Using Directed Weighted Networks : A Case Study on a Multi-Element Target Tracking Task. In *Proceedings of the Human Factors and Ergonomics Society 60th Annual Meeting* (pp. 106–110). Washington, DC, USA.

Newman, M. E. J. (2004). Analysis of weighted networks. *Physical Review E - Statistical, Nonlinear, and Soft Matter Physics*, *70*(5 2), 1–9. http://doi.org/10.1103/PhysRevE.70.056131

Opsahl, T. (2009). *Structure and Evolution of Weighted Networks*. Queen Mary College, University of London.

Opsahl, T., Agneessens, F., & Skvoretz, J. (2010). Node centrality in weighted networks: Generalizing degree and shortest paths. *Social Networks*, *32*(3), 245–251. http://doi.org/10.1016/j.socnet.2010.03.006

Opsahl, T., Colizza, V., Panzarasa, P., & Ramasco, J. J. (2008). Prominence and control: The weighted rich-club effect. *Physical Review Letters*, *101*(16). http://doi.org/10.1103/PhysRevLett.101.168702

Poole, A., Ball, L. J., & Phillips, P. (2005). In search of salience: A response-time and eye-movement analysis of bookmark recognition. In *Proceedings of People and Computers XVIII—Design for Life* (pp. 363–378). London, UK. http://doi.org/10.1007/1-84628-062-1_23

Raiha, K. J., Aula, A., Majaranta, P., Rantala, H., & Koivunen, K. (2005). Static visualization of temporal eye-tracking data. In *Proceedings of Human-Computer Interaction - Interact 2005, Proceedings* (Vol. 3585, pp. 946–949). Rome, Italy. http://doi.org/10.1007/11555261_76

Tory, M., Atkins, M. S., Kirkpatrick, A. E., Nicolaou, M., & Yang, G. Z. (2005). Eyegaze analysis of displays with combined 2D and 3D views. In *Proceedings of IEEE Visualization 2005* (pp. 519–526). Minneapolis, MN, USA. http://doi.org/10.1109/VIS.2005.37

Underwood, G., Chapman, P., Brocklehurst, N., Underwood, J., & Crundall, D. (2003). Visual attention while driving: Sequences of eye fixations made by experienced and novice drivers. *Ergonomics*, *46*(6), 629–646. http://doi.org/10.1080/0014013031000090116